Mitophagy-related prohibitin 2 is an orthoflavivirus restriction factor targeted for degradation during infection

Imanol Rodrigo[1,2,3,†], María José Romero de Ávila[1,2,3,†], Belén García-Navarro[1,2,3], Martín Arellano[1,2,3], Laura Albentosa-González[1,2,3,4], Pilar Clemente-Casares[1,2,3,4], Edward Emmott[5,#], Armando Arias[1,2,3,6,#]

Affiliation:

[1]Unidad de Medicina Molecular, Instituto de Biomedicina de UCLM (IB-UCLM), Universidad de Castilla-La Mancha (UCLM), Albacete, Spain.

[2]Unidad de Biomedicina UCLM-CSIC, Albacete, Spain.

[3]Instituto de Investigación Sanitaria de Castilla-La Mancha (IDISCAM), Spain.

[4]Facultad de Farmacia, UCLM, Albacete, Spain.

[5]Centre for Proteome Research, Department of Biochemistry, Cell & Systems Biology, Institute of Systems, Molecular & Integrative Biology, Biosciences Building, Crown Street, University of Liverpool, Liverpool, L69 7ZB, United Kingdom.

[6]Escuela Técnica Superior de Ingenieros Agrónomos y de Montes y Biotecnología (ETSIAMB), UCLM, Albacete, Spain.

Running title: Prohibitin 2 restricts flaviviral replication

Address correspondence to:

Armando Arias, armando.arias@uclm.es; Edward Emmott, e.emmott@liverpool.ac.uk

[†]These authors equally contribute to this work

Keywords: Zika, Usutu, host-virus interactions, NS5 polymerase, NS2B/NS3 protease, LGALS3BP, myoferlin, restriction factors, proviral factors.

ABSTRACT

Mitophagy selectively removes depolarised and damaged mitochondria, promoting cell viability. Some members of the *Orthoflavivirus* genus activate mitophagy to allow extended replication times in a surviving cell, while others inhibit mitophagy to favour viral spread. Viral genome replication is catalysed by non-structural protein 5 (NS5), the largest and most conserved protein in the orthoflaviviruses (OFVs). Here, we used quantitative proteomics to identify host cell interactors of Zika virus (ZIKV), Usutu virus (USUV), and West Nile virus (WNV) NS5 proteins. A total of 141 cellular interactors were found, of which 26 were common to all three NS5s. RNA interference (RNAi)-mediated knockdown of those proteins most significantly enriched revealed putative proviral and restriction activities associated. Knockdown of host myoferlin and LGALS3BP led to decreases in the virus titres, suggesting that both positively promote viral replication. Silencing of mitophagy-related prohibitin 2 (PHB2) resulted in significant increases in ZIKV and USUV titres, as well as intracellular levels of genomic RNA. Supporting a connection between this antiviral behaviour and mitophagy, an inhibitor of this pathway also led to larger virus titres and genomic viral RNA. During an infection, PHB2 protein levels gradually decreased, becoming transiently undetectable, and suggesting that it is specifically targeted and degraded by virus-mediated activities. Ectopic expression of NS5 alone did not affect PHB2 intracellular abundance, however a significant decrease was observed in cells expressing the viral protease NS2B/NS3. Its elimination, however, was more pronounced in cells where both viral enzymes were co-expressed, suggesting that NS5 could be assisting PHB2 recognition by NS2B/NS3. Overall, our results support that PHB2 is an orthoflaviviral restriction factor which is targeted for degradation to favour viral replication.

1. INTRODUCTION

Over 50 per cent of the entire human population is at risk of infection by different members of the *Orthoflavivirus* genus [1–3]. Most human orthoflaviviruses (OFVs) are transmitted by mosquitoes, with estimates suggesting that ~400 million people get infected annually, leading to >100,000 associated deaths [4,5]. The economic burden of Zika virus (ZIKV) and dengue virus (DENV) infections combined exceeds 3 billion USD annually, and 80 billion since 1975 [6]. Global warming and a broader geographic dissemination of competent vectors, among others, are factors contributing to a steady increase in the incidence and expansion of orthoflaviviral disease [4]. During the last decade, ZIKV was declared a human pathogen of international concern following large epidemic outbreaks that primarily affected the Americas and several countries in Southeast Asia. Now, the virus is present in more than 80 countries, with locally acquired cases recently documented in the EU, with estimates suggesting that 10-100 million people have been infected since the beginning of ZIKV epidemics [7–9]. Sequelae associated with infection during pregnancy can lead to severe congenital malformations, such as microcephaly, which is the most common syndrome [10]. Even though it is generally asymptomatic, ZIKV infection in adults can lead to clinical manifestations of different degree of severity, such as rash, arthralgia, conjunctivitis, meningitis, encephalitis and the Guillain-Barré syndrome [11,12].

OFVs infecting birds as their natural vertebrate hosts are an additional source of public health concern [13]. Even though humans are typically dead-end hosts for avian OFVs, neuroinvasive infection leading to severe disease occur in a significant number of cases. West Nile virus (WNV) is the most relevant avian OFV from a public health perspective, with infections in North America and Europe resulting in thousands of cases of severe disease and hundreds of fatalities associated annually [14]. Similarly to ZIKV, WNV

infection is generally asymptomatic or leads to mild-febrile illness, but one of each 100 cases results in more serious neuroinvasive disorders [15]. Usutu virus (USUV) is a new emerging threat spreading globally, and causing increasing concern. Despite being milder than WNV, a gradual increase in the number of human cases in humans and neurological disorders of varied severity linked to USUV infection has been reported [16–19]. WNV and USUV are genetically similar and exhibit serological cross-reactivity, which compromises their correct diagnosis in areas where cocirculation occur. Some evidence suggests that USUV infections in humans have been historically misdiagnosed as WNV and its true impact on public health underestimated [18,20].

The OFV genome is a positive-stranded RNA molecule which is directly translated into a single polyprotein. This polypeptide is co- and post-translationally processed by both cellular activities and the viral NS2B/NS3 protease, resulting in the release of different mature structural and non-structural proteins [21,22]. Non-structural protein 5 (NS5) contains two enzymatic activities which are critical to the synthesis and capping of new viral genomes. The RNA-dependent RNA polymerase (RdRp) domain, located in the C-terminal region, synthesises new viral RNA genome copies, whereas the N-terminal methyltransferase (MTase) domain catalyses the O- and N-methylation capping of the genomic 5' end, then required for viral RNA translation and evasion of innate immunity responses [23]. OFV replication factories are assembled inside partially secluded invaginations on the endoplasmic reticulum (ER) membranes while allowing the recruitment of cellular factors that are critical for the replication process [24–26]. These substructures ensure that replicating viral RNA is isolated from host cytoplasmic sensors. In addition to non-structural viral proteins, forty-six cellular factors have been recently identified inside these replication vesicles, most of them displaying proviral activities [24].

The use of small molecule compounds against host cell proteins necessary for viral replication has emerged as an attractive field in antiviral research [27,28]. In addition to its central activity in genome replication, NS5 has been revealed as a multifaceted protein, engaging in diverse processes that include suppression of innate immunity, transcription reprogramming, and interference with normal cell cycle progression [29–31]. Several NS5 cellular partners have already been identified, including proviral activities [24,28,32–35] and restriction factors, such as those in the JAK-STAT pathway [36–38].

Mitophagy is a type of selective autophagy to remove irreparably damaged or depolarised mitochondria and promote cell survival. Since damaged mitochondria can activate innate immunity and proinflammatory responses, many viruses modulate mitophagy in an infected cell [39]. When this pathway is activated, PINK1 is accumulated in the outer mitochondrial membrane (OMM), leading to the recruitment of E3-ubiquitin ligase Parkin [40]. Parkin ubiquitylates different OMM proteins, attracting other factors needed to initiate mitophagy [41]. The mitochondrial fusion-fission cycle critically affect mitophagy, since impaired mitochondria fission blocks mitophagy activation [42]. Prohibitin 2 (PHB2), a multitasking protein found in several subcellular locations, has been recently identified as a mitophagy receptor [40,43]. PHB2 interacts with SQSTM1 and LC3 in the inner mitochondrial membrane to drive damaged mitochondria to the autophagosome [44].

Evidence support that mitophagy is actively modulated by OFVs during infection [45]. The activation of mitophagy is critical for Japanese encephalitis virus (JEV) replication in a hepatoma cell line and is also necessary in cells persistently infected with hepatitis C virus (HCV), closely related to OFVs [46,47]. Mitophagy is however silenced during DENV infection, leading to an accumulation of damaged mitochondria and cellular injury [48]. For ZIKV, mitophagy activation has been associated with both proviral and antiviral activities

[45]. Ponia and colleagues demonstrated that ZIKV supresses mitophagy in astrocytes, in a process where NS5 interacts and interferes with host protein Ajuba [49]. While no overall effect was observed on viraemia, Ajuba knockout (KO) mice showed larger viral loads in tissues, and also an increase in proinflammatory cytokines and interferon β (IFN-β), supporting that mitophagy inhibition and enhanced inflammatory responses promote virus dissemination [49]. By contrast, Lee and Shin found that mitophagy inhibition, through RNAi-mediated PINK1 silencing, repressed viral replication, suggesting that mitophagy is distinctly regulated by different OFVs and/or cellular contexts to maximise virus infection and propagation [45,50].

In the present study, we identified 141 host factors that interact with the NS5 proteins of ZIKV, WNV, and USUV. We found that 26 of these factors were common interactors for all three NS5s, including PHB2. PHB2 gene silencing led to increases in both virus titres and genomic RNA, supporting that this protein may act as a restriction factor. During both ZIKV and USUV infection, PHB2 abundance gradually decreased, becoming transiently undetectable in the infected cultures, and supporting that OFVs specifically target PHB2 to promote viral replication. Ectopic expression of NS2B/NS3 protease but not NS5 led to PHB2 degradation. PHB2 was eliminated more efficiently by NS2B/NS3 when NS5 was co-expressed in the same cells, supporting that NS5 may be assisting the viral protease in the recognition and subsequent degradation of PHB2. In the study, we identified other NS5 interactors that were critical to virus infection, such as myoferlin (MYOF) and LGALS3BP, encouraging the use of specific drugs as potential therapeutics.

2. MATERIALS AND METHODS

2.1. Cells, viruses, and protocols for infections

The origin of ZIKV and USUV strains has been detailed in previous manuscripts [33,51,52]. For virus infections, A549 (adenocarcinoma human alveolar cell line), Huh7.5 (human hepatoma cells), HEK 293T (human embryonic kidney cells expressing SV40 T-antigen), and Vero (African green monkey kidney epithelial cell line) cells were used as previously described [33,53]. All the cells were grown in complete media containing either 5% (Vero) or 10% (293T, Huh7.5, A549) (v/v) foetal bovine serum (FBS, Sigma or Cytiva) and 100 units/ml penicillin-streptomycin (Gibco) in high-glucose DMEM (Gibco). Huh7.5, A549 or 293T cells media were supplemented with 2 mM L-glutamine (Gibco). Vero cells media contained 1 mM HEPES pH 7.0.

Infections were carried out as described in previous manuscripts [33,54]. Briefly, the day before virus inoculation 2 x 10^4 or 1 x 10^5 cells were seeded in either 96-well or 24-well plates, respectively, in the presence of complete media, and incubated overnight at 37°C with 5% CO_2. On the next day, cell supernatants were removed and replaced with high-glucose DMEM containing 1% FBS and 100 units/ml penicillin-streptomycin. Virus was applied at the multiplicity of infection (MOI) indicated, and adsorption allowed for 1 hour. The inoculum was removed, and the cells washed to eliminate unattached virus. Cells were then covered in media containing 1% FBS. The supernatants and/or cell lysates were collected at different time points for subsequent virus titration by 50% tissue culture infectious dose ($TCID_{50}$) assays, RNA extraction and quantification (qPCR) or Western blot analysis.

2.2. Virus titration assays

Viral samples were titrated by $TCID_{50}$ assays, using protocols that have been previously described [32,33,51]. To this, 10^4 Vero cells in 60 µl of media containing 5% FBS were seeded into 96-well plate wells. On the next day, 100 µl of 10-fold serial dilutions of each

virus in media containing 1% FBS were applied to wells, reaching a final volume of 160 µl. The virus titres were determined at day 4 (USUV) or 5 (ZIKV) post-infection by scoring the number of infected wells showing apparent cytopathic effect [55,56].

2.3. Gene silencing with Dicer-substrate small-interfering RNAs (DsiRNAs)

To achieve specific host gene silencing, we used DsiRNA duplexes purchased from Integrated DNA Technologies (IDT). Information regarding the host gene-target sequence has been provided as supplementary information (Supplementary Table S1). As a negative control, a DsiRNA with no human genome target, namely NonSP, was used. To specifically silence each host factor, 5 pmol of each DsiRNA were added into each well of a 96-well plate, in the presence of 0.25 µl of lipofectamine RNAiMAX (Invitrogen) and 50 µl of opti-MEM (Gibco), as suggested by the manufacturers. The mix was incubated for 20 minutes to allow the formation of RNA-lipofectamine complexes, and then 1.5 x 10^4 A549 cells were seeded on top. Twenty-four hours after transfection, the cellular supernatants were removed, and virus was inoculated at an MOI of 0.1 or 1 $TCID_{50}$/cell. Following virus adsorption during 1 h at 37 °C, the inoculum was removed, cell monolayers washed, and fresh media containing 1% FBS added. Virus titres and genomic RNA levels in the supernatants and/or attached cells were determined by $TCID_{50}$ or qPCR assays as detailed elsewhere.

2.4. Drug treatment and cell viability assays

Host targeting drugs WJ460 [3-(3-(2-methoxyphenyl)-4-oxo-2-thiazolidinyl)-N-(4-phenylbutyl) benzamide] and mdivi-1 [3-(2,4-dichloro-5-methoxyphenyl)-2-mercaptoquinazolin-4(3H)-one] were purchased from MedChemExpress. The number of metabolically live cells after exposure to these compounds relative to mock-treated cultures, or after transfection with different host-targeting DsiRNA molecules relative to

negative control DsiRNAs (not recognising human sequences) were obtained by using the *CellTiterBlue* kit (Promega), as previously described [32,33].

2.5. Viral RNA extraction and quantification by quantitative PCR (qPCR)

Total RNA was extracted from whole cell monolayers grown in 96-well plates, using NZY Total RNA Isolation kit (NZYtech). To quantify ZIKV or USUV genomic RNA in the sample, we used different sense and antisense primers, and a FAM-TAMRA probe. ZIKV RNA was detected with a probe targeting the ZIKV E gene (positions 1214 to 1244), and primers spanning positions 1192 to 1208 and 1269 to 1246, while USUV RNA was quantified using a probe targeting USUV NS1 gene (positions 3322 to 3345), and primers spanning positions 3288 to 3309 and 3372 to 3351, all purchased from IDT. To amplify and detect both ZIKV and USUV genomic RNA, we used NZYSupreme One-step RT-qPCR Probe Master Mix (2x), ROX kit (NZYtech), and RT-PCR conditions as indicated by the manufacturer, with a reverse-transcription step (15 min at 50ºC), followed by 3 min of incubation at 95°C and 40 amplification cycles of 5s at 95°C and 45s at 60°C. To obtain a standard curve containing known amounts of ZIKV and USUV RNA, 4µl of whole cell RNA purified from infected cultures was reverse transcribed in 20µl final volume using SuperScript III Reverse Transcriptase (Invitrogen). Then, 3µl of cDNA were PCR-amplified using Phire Hot Start II DNA Polymerase (Thermo Fisher Scientific), and primers spanning residues 949 to 967 (forward) and 1934 to 1915 (antisense) for ZIKV, and 2809 to 2829 (forward) and 3808 to 3787 (antisense) for USUV. Both forward primers included a T7 promoter preceding the ZIKV or USUV homology region. PCR amplicons were then purified, using NZY GelPure kit (NZYtech), and ligated into the PCR Blunt plasmid using the *Zero Blunt PCR cloning* kit (ThermoFisher). Linearised plasmids containing the inserts, or directly the PCR amplicons abovementioned, were in vitro transcribed with the *mMESSAGE mMACHINE T7 Transcription* kit (Ambion) following the protocols

recommended by the provider. After DNAse treatment, the RNA transcript was purified and quantitated, using a Nanodrop spectrophotometer. The standard curve samples were prepared by 1:10 serially diluting in vitro transcribed RNA into precise number of molecules (from 10^8 to 10^1 viral RNA molecules/µL) in 100 ng/µl yeast RNA.

2.6. Relative quantification of host mRNA transcripts by qPCR

To confirm host gene knockdown after DsiRNA transfection, RNA was extracted from cells, using the NZY Total RNA Isolation kit (NZYTech), as described above. Host gene mRNA levels were determined by using the *One-step NZYSpeedy RT-qPCR Green kit, ROX* kit (NZYtech) in a CFX Duet Real Time PCR instrument (BioRad) with specific primer pairs, all provided by IDT [reference numbers (Hs.PT.58.): 27059869, 19355804, 40826680, 2219540, 3098270, 40209489, 456578.g, 3838519.g, 38465792, 22859503, 22973334, 27422678.g, 40506149, 40261049]. As a reference we used primers amplifying a housekeeping gene (Hs.PT.39a.22214836 for GAPDH). The efficiency of each transcript downregulation was calculated following the $2^{-\Delta\Delta CT}$ method [33,57]. To the detection of IFN-β overexpression in experiments involving virus-infected or poly I:C stimulated cells, a primer set from IDT to detect host IFNB1 mRNA transcript was also purchased (Hs.PT.58.39481063.g).

2.7. Poly I:C treatment and detection of IFN-β overexpression

To analyse the effect of PHB2 downregulation on IFN-β expression, A549 cells were transfected with different amounts of poly I:C [Poly (I:C) (LMW), Invivogen], using Lipofectamine 3000 in the absence of the P3000 reagent (Invitrogen). Twenty-four hours prior poly I:C stimulation, cells were transfected with DsiRNAs (either targeting PHB2 or a control sequence with no target on the human genome), as explained above. Poly I:C

stimulated cells were then collected at different intervals, and total cell RNA extracted as mentioned above, to analyse IFN-β gene transcription along time (relative IFNB1 mRNA).

2.8. Vectors and mutagenesis

To the expression of ZIKV, USUV, and WNV polymerases in mammalian cells we are using constructs previously prepared in our group [32,58]. Specifically, HA-tagged versions of the full NS5 (HA-NS5) or the RdRp domain alone (HA-RdRp) of each viral protein were inserted into a pcDNA3 vector [32,33]. A vector expressing ZIKV RdRp domain (amino acids 267 to C-t) fused to an HA tag and EYFP in its N- and C-termini (pZIKV-HA-RdRp-EYFP), respectively, was also prepared. To this, the RdRp domain of ZIKV NS5 (fused to an N-terminal HA tag) was PCR shuffled with the EYFP gene from pEYFP-N1 (Clontech), including a 5x Gly linker between both sequences. The amplicon was then cloned into pcDNA3, using EcoRI and XhoI restriction sites.

To the expression of ZIKV NS2B/NS3 protease, we swapped the HA-RdRp-EYFP coding region in the plasmid mentioned above (pZIKV-HA-RdRp-EYFP) by the corresponding NS2B3-coding region, using the *In-Fusion HD EcoDry Cloning Kit* (Takara Bio). To this, the vector was first amplified with a specific reverse primer 5'-AGCGTAATCTGGAACATCGTATGGGTA-3', located immediately before the gene insert but including the HA-tag region, and a forward primer 5'-GATAACTCGAGCATGCATCTAGAG-3', spanning the region located immediately after the gene insert and a Stop codon. This resulted in the amplification of the linearised vectors devoid of any insert, but including the sequence for an N-terminal HA tag. To the amplification of the NS2B3 coding region we used a forward primer spanning ZIKV genomic positions 4224 to 4244 and a reverse primer complementary to positions 6464 to 6444. Both primers contained 15-nt tails overlapping with the linear amplicon generated

above. Both vector and NS2B3 amplicons were ligated by recombination, leading to the pZIKV-HA-NS2B3 plasmid.

The presence of the correct expression cassette in both pZIKV-HA-RdRp-EYFP and pZIKV-NS2B3 was confirmed by Sanger sequencing. All plasmids used in this study have been transfected into HEK 293T, A549 or Huh7.5 cells with either the *Lipofectamine 3000 kit* (Invitrogen) or the *FuGENE 4K* reagent (Promega), using the instructions provided by the manufacturers.

2.9. Co-immunoprecipitation and mass spectrometry methods

HEK 293T or A549 cells were lipofected with plasmids expressing full-length ZIKV, USUV or WNV NS5 proteins (HA-NS5) or their RdRp domains (HA-RdRp or HA-RdRp-EYFP). At 24 to 48 h post-transfection, cells were scrapped on ice-cold PBS, and spun at 300x *g* for 5 min, washed in PBS twice, and the pellet resuspended at 4°C in 450 µl of RIPA buffer (10 mM Tris-HCl pH 7.5; 150 mM NaCl; 0.5 mM EDTA; 1% SDS; 1% Triton X-100; 1% deoxycholate) in the presence of 1x protease inhibitor cocktail (Complete Mini EDTA-free protease inhibitor cocktail, Merck) and 250 U/ml benzonase (Sigma). To remove the cellular debris, the lysate was then spun during 10 mins at 15000x *g* and the resulting supernatant was recovered. To ensure that each co-IP assay contained the same amount of lysate, protein concentration in each sample was determined with the *BCA Protein Assay Kit* (Pierce) and then normalised to a final volume 400 µl in RIPA buffer. The samples were then equilibrated in 1.5 volumes (600 µl) of dilution buffer (10 mM Tris-HCl pH 7.5; 150 mM NaCl; 0.5 mM EDTA). Anti-GFP agarose beads (protag-HiPur GFP, Progen) or anti-HA agarose or magnetic beads (Pierce) were pre-equilibrated in 1x dilution buffer, and then added to the lysates. The mix was incubated in a rotary shaker overnight at 4ºC. The beads were then either magnetically separated (magnetic beads) or pelleted

by centrifugation (agarose beads), the supernatant eliminated, and then washed four times in wash buffer (1x dilution buffer containing 0.05% Nonidet P40 substitute, Fluka BioChemika). Finally, the co-IP proteins were released by resuspending the beads in 1x Bolt LDS Sample Buffer (Life Technologies), 1x RIPA buffer, and boiling at 90°C for 5 min.

For the identification of host cell interactors by mass spectrometry, full-length versions of ZIKV, USUV and WNV NS5 proteins were expressed in A549 cells followed by co-immunoprecipitation (co-IP), using anti-HA magnetic beads, as described above. The pulldowns were SP3-precipitated [59], trypsin digested and labelled with TMTpro. LC-MS/MS was performed on a Dionex U3000 UHPLC, in-line with a Q-Exactive-HF mass spectrometer as described previously [60]. Data were analysed with MaxQuant 1.6.7.0 [61]. N-terminal protein acetylation and methionine were set as variable modifications, enzyme specificity was set to trypsin with up to two missed cleavages. Data were searched against fasta files containing the Swissprot human proteome entries (20,300 entries, downloaded 2020/03/12) and a custom fasta file containing the HA-tagged NS5 sequences. For each NS5, four independent transfections, co-IPs were performed, one control was removed at the data analysis stage as an outlier. To identify those factors that were significantly enriched in the IPs, four independent plates were mock-transfected in parallel with an empty vector (pcDNA3). NS5-interacting factors were identified using the *Perseus software* version 2.0.6.0., as previously described [62]. A list with all host factors that are significantly enriched in ZIKV, USUV and WNV HA-NS5 co-IPs followed by TMT-based proteomics are provided as supplementary material (Supplementary Tables S2 – S4). The mass spectrometry data, including .fasta files has been submitted to proteomeXchange via the PRIDE repository and has accession number PXD071636.

2.10. Western blot analysis

To the detection of host and virus protein in infected cells or transient expression of recombinant cells, we followed protocols previously described [33]. Briefly, 50 µg of cell protein lysates were resolved in SDS-PAGE electrophoresis, and transferred to an Immobilon-P PVDF membrane (Millipore). The membranes were blocked in 10% non-fat dry milk in 1x Phosphate Buffered Saline (PBS) containing 0.05% Tween-20 (PBS-T) and incubated in the presence of the corresponding primary antibody (1:500 dilution in 4% non-fat dry milk), following protocols previously described [32,33]. Primary antibodies used for Western blot include mouse anti-HA epitope (BioLegend, reference 901501), rabbit anti-FLAG epitope (Proteintech, reference 20543-1-AP), rabbit anti-PHB2 (Invitrogen, PA5-21417), rabbit anti-STAT2 (Cell Signaling, 72604S), rabbit anti-ZIKV NS3 (Invitrogen, PA5-143436) and rabbit anti-ZIKV NS5 (Genetex, GTX133328). As loading controls, HRP-conjugated antibodies against GAPDH (Genetex, GTX627408-01) and tubulin (Cell Signaling, 12351S), not requiring secondary antibody to detection, were also used.

2.11. Gene ontology analysis

Gene Ontology (GO) enrichment analysis was performed on differentially abundant proteins (FDR < 0.05) in the pulldowns using g:Profiler with the Benjamini-Hochberg correction. Redundant GO Biological Process (BP) terms were reduced using rrvgo (v1.10.0) with a Wang semantic similarity threshold of 0.7. GO Cellular Component (CC) terms with <5 genes were excluded from the analysis. Remaining terms were grouped only when sub-compartments shared a parent GO category (e.g., mitochondrial compartments) and the combined gene count remained statistically robust (≥5 genes). A summary of all enrichment analysis to the identification of BP and CC terms are provided as supplementary material (Supplementary Tables S5 and S6).

2.12. Statistical analysis

Statistical significance was determined using *GraphPad Prism 8* and different statistical tests as specified in each corresponding figure legend.

3. RESULTS

3.1. Identification of host factors associated with orthoflaviviral NS5s

Full-length versions of ZIKV, USUV and WNV NS5 proteins were expressed in A549 cells, and their interacting host cellular factors isolated as described in the Methods section. Mass spectrometry analyses resulted in the identification of 72, 63 and 77 cellular proteins significantly enriched in pulldowns of ZIKV, USUV and WNV NS5s, respectively (Figure 1, Supplementary Tables S2 – S4). The GO enrichment analysis revealed that most of them were either involved in biological processes that were related to the metabolism of RNA (RNA splicing and processing), ribosome biogenesis and protein translation, chromatin assembly and chromosome organisation, or aerobic respiration and proton transport in the mitochondria (Figures 1 and 2, Supplementary Figure 2). The intersection of the three sets (ZIKV, WNV, USUV) identified 26 proteins that were found in all co-IPs (Figure 1A, Supplementary Figure S2). To the identification of those interacting factors that could be more biologically relevant to the OFVs, we re-examined the intersection, but using only the top 50 significantly enriched proteins in each pulldown. This resulted in 14 host factors present in all three sets (Figure 2, Supplementary Tables S2 – S4). Most of the host factors identified in the intersection are mitochondrial proteins (ATP5B, PHB2, PGAM5, FH and SFXN1) or participate in ribosome biogenesis and/or protein translation (RSL1D1, RPL21, RPL24, RPL24).

3.2. Silencing of NS5 host partners identifies proviral and restriction activities

To examine the biological impact of these 14 host factors to OFVs, we assessed how their silencing affected viral replication, using specific DsiRNAs against them (Figure 3). All DsiRNAs used in our study caused efficient downregulation, with over 70% reduction in each mRNA transcript compared to controls transfected with a non-specific DsiRNA (Supplementary Figure S3). Except for ribosomal proteins RPL21, RPL24 and RPL34, gene silencing had no effect or caused only a modest decrease in cell viability at 48 h post-transfection, with more than 75% live metabolically active cells for all factors studied (Supplementary Figure S4). Downregulation of either PHB2 or ribosomal L1 domain-containing protein 1 (RSL1D1) resulted in larger virus titres in the supernatant of both ZIKV- and USUV-infected cells, suggesting these two proteins are restriction factors for the OFVs (Figure 3). Downregulation of RPL21, PGAM5, SFXN1 and SMARCA5 also led to significant increases in USUV but not in ZIKV titres, while DDX21 silencing resulted in increased ZIKV but not USUV infectivity.

Silencing of LGALS3BP and MYOF significantly affected both ZIKV and USUV replication, with pronounced losses in virus titres, supporting that these are proviral proteins (Figure 3). To confirm this possibility, we examined the effect of their downregulation at different time points and MOIs, finding similar results to those obtained before (Figure 4, Supplementary Figure S5). Viral replication was significantly impaired when MYOF was silenced, with 1,000- to 10,000-fold decreases in virus titres at 72 h post-infection (Figure 4). MYOF downregulation modestly affected the relative amount of metabolically active cells (>80%) at 48 h post-transfection (Figure 4), supporting that the detrimental effect on viral replication is specifically related to gene silencing and not to losses in viability. Since MYOF seems to be critical to virus replication, we investigated whether it represents a

suitable target for therapeutic molecules. To this, we examined the effect of a MYOF inhibitor (WJ460) on virus infection. Although WJ460 specifically inhibits all known MYOF cellular functions [63], we observed only a modest inhibition on ZIKV titres (~1-log10 reduction), and no effect on USUV. This apparent lack of antiviral activity was observed even at concentrations causing significant cell toxicity (40 to 160 μM), in contrast to data obtained with DsiRNAs (Fig 4E – 4G).

3.3. PHB2 downregulation stimulates orthoflaviviral replication

Since the preliminary DsiRNA-based screening identified PHB2 and RSL1D1 as putative orthoflaviviral restriction factors (Figure 3), we further examined how their silencing affected virus replication (Figure 5, Supplementary Figure S6). In agreement with our previous observations, significant increases in ZIKV and USUV titres were found at different time points and MOIs when these host genes were knocked down. Given that mitophagy modulates OFV infection, and PHB2 acts as receptor of such pathway, we further analysed the effect of this protein to the virus life cycle. We found that PHB2 silencing also led to significant increases in intracellular viral RNA in both ZIKV- and USUV-infected cells (Figure 5G-5J). PHB2 downregulation was also accompanied with increased NS5 protein levels during ZIKV infection, further supporting that PHB2 restricts viral replication (Figure 5B, Supplementary Figure S7). To examine whether larger titres and RNA levels could be related to an increase in virus particle release, we compared extracellular to intracellular viral RNA ratios in PHB2-depleted and unspecific DsiRNA-targeted cells (Supplementary Figure S8), but no significant differences were found. This observation may indicate that larger virus titres and genomic RNA in PHB2-depleted cells may be the result of enhanced genome replication. Thus, PHB2 could be acting as an OFV antagonist, being favoured viral genome synthesis in its absence.

To assess whether the connection between PHB2 silencing and increased viral replication could be related to mitophagy, we used mdivi-1, an inhibitor of mitochondrial fission-related protein DRP1 which also represses mitophagy [64]. We confirmed that treatment with 10μM mdivi-1 resulted in both larger ZIKV titres and genomic RNA copies (Figure 6), as observed in PHB2-downregulated cells by RNAi (Figure 5). Accordingly, larger virus titres were also detected in USUV-infected cells treated with mdivi-1 (Supplementary Figure S9).

3.4. PHB2 is transiently eliminated during infection

To further examine its biological relevance during the orthoflaviviral life cycle, we analysed PHB2 protein level kinetics in infected cultures (Figure 7). We found that PHB2 intensity gradually decreased to become barely detectable at 48 h post-infection (< 5% relative to mock-infected cells) in both ZIKV- and USUV-infected A549 cells (Figure 7). At later time points, PHB2 was again detected at intensity levels similar to those in control uninfected cells (101-145% in ZIKV and 58-69% in USUV, respectively). PHB2 signal was also transiently reduced during infection in 293T cells, supporting that this protein is specifically targeted for degradation or its expression is repressed in different human cell types (Figure 7H). No significant variations in the relative amount of PHB2 mRNA transcripts in mock- and virus-infected cells were found (Supplementary Figure S10), conveying that reduced protein levels may be due to degradation, rather than to reduced transcriptional levels. Virus titres in A549 cells plateau at 36 h post-infection (Supplementary Figure S10), and hence reduced PHB2 levels in the 36 to 48 h post-infection interval may be directly related to enhanced viral genome replication and/or particle assembly prior to release.

3.5. PHB2 depletion correlates with larger interferon levels in infected cells

PHB2 together with prohibitin 1 (PHB1) have been proposed as major contributors to the

MAVS-mediated antiviral signalling against cytoplasmic viral RNA, leading to the activation of type I interferon (IFN-I) responses [65]. Since PHB2 is transiently eliminated during infection (Figure 7), we pondered that its degradation may be interfering with MAVS-signalling cascade. To assess this possibility, we analysed IFN-β gene (IFNB1) transcription levels in cells where PHB2 had been previously knocked down. For both ZIKV and USUV, we found larger IFNB1 mRNA levels in PHB2-depleted cells than in cultures transfected with a non-specific DsiRNA (Figure 8A – 8D), in contrast with previous observations [65]. Since PHB2 downregulation stimulates viral replication, resulting in larger numbers of viral RNA genome copies, enhanced IFNB1 mRNA transcription could be incidental rather than directly prompted by PHB2 depletion. To evaluate this possibility, we quantitated the relative amount of IFNB1 mRNA in cells stimulated with poly I:C, a non-replicating double-stranded RNA molecule. Although modestly, we also found that PHB2 silencing resulted in significant increases in IFNB1 mRNA levels (Figure 8E – 8H). To further explore whether IFNB1 transcription activation was connected to mitophagy inhibition, we analysed mRNA levels in ZIKV-infected cells treated with mdivi-1 but, in this case, IFNB1 mRNA levels were moderately lower in the presence of the inhibitor (Figure 6D).

3.6. NS5 stimulates PHB2 degradation by the viral protease NS2B/NS3

Since host STAT2 degradation by the proteasome is directly mediated by NS5 in ZIKV and DENV [36,38], and that NS5 specifically interacts with PHB2 (Figure 2), direct PHB2 degradation by NS5 was a plausible scenario. Coincidentally, ZIKV NS5 and host PHB2 protein levels both decrease at 48 h post-infection when compared to the previous data points (Figure 7A – 7D). We first confirmed that PHB2 and NS5 proteins interacted in co-IP assays followed by Western blot (Figure 9A), as previously inferred from our mass spectrometry data (Supplementary Tables S2 – S4). PHB2 was also pulled down when the

RdRp alone was used as a bait, supporting that NS5 interacts with this cellular protein through the polymerase domain (Figure 9B). To assess whether NS5 expression and PHB2 degradation were linked, we used increasing amounts of all three NS5 expression constructs, but no significant changes in PHB2 detection were found (Figure 9C, Supplementary Figure S11). Nonetheless, we confirmed that our ZIKV NS5 construct resulted in efficient STAT2 downregulation when transfected, as previously documented (Figure 9C, Supplementary Figure S11).

Since NS5 seemed not to be directly leading to PHB2 degradation, we anticipated that other viral factors might be involved. In addition to viral polyprotein maturation, the orthoflaviviral protease NS2B/NS3 also participates in the recognition and proteolytic cleavage of different cellular proteins during infection [66–68]. Thus, we examined the effect of ZIKV NS2B/NS3 on PHB2, confirming that the ectopic expression of its precursor (NS2B3) resulted in decreased protein levels (Figure 9D). To examine a possible synergistic activity of both viral proteins, we analysed the effect of NS5 coexpression in cells transfected with a suboptimal amount of the pZIKV-NS2B3 construct. We confirmed that the expression of viral NS2B/NS3 is accompanied by a decrease in PHB2 abundance, and that this reduction is enhanced in the presence of NS5 (Figure 9E and 9F). These observations support that both viral proteins participate in the recognition of PHB2 and its subsequent degradation.

4. DISCUSSION

Owing to its central role to the virus life cycle, here we seek to examine the interacting networks of orthoflaviviral NS5 within the host cell in full detail. We deem that this information can be instrumental in advancing our understanding on the virus-cell interactions directly engaging in viral genome replication and diverse processes affected

by NS5. Mitophagy has attracted attention as a key cellular process modulating orthoflaviviral infection [49,50]. In this manuscript, we have identified PHB2, a mitophagy receptor, as a restriction factor for OFV replication. RNAi-mediated PHB2 silencing resulted in increased viral titres, genomic RNA and protein translation, sustaining our hypothesis (Figure 5). We have found that mdivi-1, a mitophagy inhibitor, also promotes higher virus titres in infected cells, supporting a relationship between this restriction activity associated with PHB2 and this cellular pathway [64,69]. Previous studies established a connection between ZIKV NS5 and mitophagy inhibition [49]. NS5 binds to host protein Ajuba, preventing its translocation to depolarised mitochondria and supressing PINK1-mediated mitophagy activation. In our study, while a connection between PHB2 and viral replication has been established, it remains to be further examined how its degradation, observed in infected cells, affects mitophagy. In addition to PHB2, we have identified other mitochondrial proteins as NS5 interactors, such as PGAM5 which also plays an important role during mitophagy [40,70], several subunits of the mitochondrial ATP synthase (e.g. ATP5F1B), fumarate hydratase (FH) and sideroflexin-1 (SFXN1). These findings are suggestive of mitochondria dynamics playing a crucial role during OFV infection, and of NS5 as a factor subverting some cellular processes controlled by these organelles.

Besides mitochondria, PHB2 can also be found in different subcellular locations, including the nucleus, cytosol and plasma membrane, engaging in various signalling pathways in cell metabolism, migration and proliferation [71]. A conceivable situation is that viral restriction by PHB2 is connected to other cellular processes, in addition to mitophagy. The translocation of PHB2 into the nucleus interferes with long-noncoding RNA and gene transcription, acting as a repressor of diverse transcription factors such as MyoF and MEF2 transcription factors, and the oestrogen receptor [72–75]. Evidence suggests that oestrogen-dependent signalling could elicit a proviral activity, since inhibition by tamoxifen

also inhibits orthoflaviviral replication [76]. Thus, a tantalising possibility is that PHB2 antiviral activity operates at the transcriptional level, and its absence exerts a proviral effect, connected to ESR-signalling activation [76–78].

PHB2 is transiently eliminated during ZIKV or USUV infection in different cell contexts, suggesting that its degradation is critical to the virus life cycle (Figure 7). Since both ZIKV and DENV NS5 proteins target STAT2 to proteasomal degradation, we initially considered that PHB2 elimination might be caused by NS5. In the case of STAT2, NS5 acts as a protein bridge between this protein and an E3 ubiquitin ligase, leading to STAT2 degradation in a ubiquitin-dependent process [36,38]. We have recently documented that OFV NS5s also interact with UBA1, the primary E1 ubiquitin-activating enzyme in most ubiquitylation events [33]. However, we found that the ectopic expression of NS5 alone does not affect PHB2 protein levels, being required the viral protease NS2B/NS3 to its degradation (Figure 9D). Nonetheless, the amount of PHB2 gradually decreases in the presence of increasing amounts of NS5 when a suboptimal amount of the pZIKV-NS2B3 construct is used (Figure 9E and 9F). A physical interaction between NS5 and the C-terminal domain of NS3 has been documented, and hence this could also be taking place between NS5 and the NS2B/NS3 complex [79,80]. Our current hypothesis is that NS5 facilitates the interaction between PHB2 and the viral protease, enabling its subsequent degradation. If this is correct, NS5 could be acting as a protein bridge, not only for PHB2 elimination, but also for other restriction factors. In addition to degradation, a possible alternative is that NS5 could be sequestering PHB2 and thus interfering with other cellular processes. Several lines of evidence support that orthoflaviviral NS5s can interfere with host factors of the IFN-I-dependent JAK-STAT signalling pathway, such as IKKε and TBK1 [31,81,82].

Previous studies have established a connection between PHB2 and MAVS-mediated antiviral signalling. Therefore, a forthcoming explanation would be that OFVs targeting PHB2 to degradation might help uncouple MAVS activation from IFN-I production [65]. MAVS is activated when replicating viral RNA in the cytoplasm is detected by retinoic acid inducible gene type I (RIG-I) – like receptors (RLRs), such as RIG-I and MDA5. Activated RLRs interact with MAVS in the mitochondrial membrane, triggering the downstream signalling pathways that lead to the production of IFN-I and proinflammatory interleukins [83,84]. Our data suggest however that PHB2 knockdown during infection activates IFN-I transcription, in contrast with previous observations [65]. We observed larger IFNB1 levels in both infected or poly I:C stimulated cells when PHB2 was silenced (Figure 8). Yoshinaka and colleagues found that downregulation of either PHB1 or PHB2 resulted in decreased IFN-β levels after infection with Sendai virus (SeV) or poly I:C stimulation stimulation with (Yoshinaka et al., 2019). These differences could be, at least in part, attributed to the use of different cell lines, or to the fact that an infection by a positive (OFV) or a negative-stranded (SeV) RNA virus could trigger distinct responses. Further analysis is needed to better understand the possible connection between MAVS and PHB2 in the context of an orthoflaviviral infection.

Larger IFNB1 transcription levels observed in PHB2-silenced cells seems counterintuitive to the antiviral role that we are claiming for this host protein (Figure 8). This could be partially explained in the context of fluctuating PHB2 abundance observed in the infected cells. We hypothesise that transient PHB2 degradation observed at 48 hpi could be leading to enhanced viral RNA genome replication (Figures 5 and 7). Subsequent PHB2 restoration to normal levels at 60 hpi could be triggering mitophagy activation (Figure 7), thereby preventing exacerbated inflammation and hence attenuating the ensuing MAVS antiviral response [69,85]. Several studies have documented the role that mitophagy in

maintaining innate immunity homeostasis, by modulating the cellular inflammatory responses, in agreement with our hypothesis [86–89].

In the study we also identified other NS5 partners affecting orthoflaviviral replication. Larger virus titres were recovered in both ZIKV- and USUV-infected cells when RSL1D1 was silenced, also supporting an antiviral activity associated with this host factor (Supplementary Figure S6). RSL1D1 is an RNA-binding protein participating in multiple cellular processes, including antagonising senescence, proliferation and apoptosis, and acting as an autophagy suppressor in different types of cancer [90,91]. Conversely, MYOF and LGALS3BP downregulation led to significant decreases in both ZIKV and USUV titres, suggesting that both factors contribute to critical steps of the life cycle (Figure 4, Supplementary Figure S4). MYOF is a multifunctional Ca2+ – binding protein which, besides vesicle trafficking regulation, participates in endocytosis-induced membrane repair activities [92,93]. Since OFVs assemble their replication sites in ER membrane invaginations requiring extensive remodelling, it is conceivable that membrane-repair activities might be relevant to their formation [94]. WJ460, a promising anticancer drug targeting MYOF Ca2+ – binding C2D domain [92,95], showed only a minor effect on virus titres, in contrast with DsiRNA-mediated silencing (Figure 4). Despite human MYOF cryo-EM structures have been recently solved, attempts to obtain a complex with WJ460 remain elusive [95]. Additional studies suggest that WJ460 may target different other host factors, and thus its inhibitory effects not being totally associated with MYOF [96].

LGALS3BP is a secreted glycoprotein that has been associated with immune modulation, tumour progression, and extracellular matrix organization. During infection, LGALS3BP is activated, leading to increased IFN production and proinflammatory responses [97]. WNV infection in mice results in the upregulation of LGALS3BP in the CNS [98]. However, while

KO mice showed reduced neuroinflammation, increased microglial numbers, and alterations in T cell populations, no significant differences in WNV replication titres are observed [98]. This evidence suggests that LGALS3BP is not critical to WNV infection in mice, in contrast to our data with ZIKV and USUV in cell culture.

In addition to advance our understanding of the OFVs biology, we deem this study open new avenues for their therapeutic control. Approaches based on stimulating PHB2 antiviral activity or, alternatively, molecules triggering mitophagy activation, which are expected to antagonise viral replication, could be considered in future studies. The identification of the interacting epitopes between NS5 and its cellular counterparts could also be instrumental in the rational design of antivirals disrupting their binding interfaces.

ACKNOWLEDGEMENTS

We thank José Joaquín Lorenzo for his technical assistance to this work.

FUNDING INFORMATION

This research was supported by grant SBPLY/24/180225/000240, from Junta de Comunidades de Castilla-La Mancha (JCCM), awarded to AA and LAG. AA is also the recipient of grants PID2022-137974OB-I00 and CNS2022-135258 from Ministerio de Ciencia, Innovación y Universidades (MICIU/AEI/10.13039/501100011033) and FEDER (EU), and grants SBPLY/21/180501/000076 and SBPLY/24/180225/000240 from Junta de Comunidades de Castilla-La Mancha (JCCM). Work in AA's lab is also supported by core funding from UCLM (grant numbers 2025-GRIN-38349 and 2022-GRIN-34150). IR and MJRdA are, respectively, the recipients of fellowships 2020-PREDUCLM-16723 and 2024-INVGO-12348, both granted by UCLM. Research in EE's lab is supported by an AMS Springboard Award (SBF006\1008) funded by the Academy of Medical Sciences (AMS),

the Wellcome Trust, the Government Department of Business, Energy and Industrial Strategy (BEIS), the British Heart Foundation and Diabetes UK, an MRC NIRG (MR/X000885/1) and Wellcome Career Development Award (227831/Z/23/Z).

FIGURE LEGENDS

Figure 1. Summary of orthoflaviviral NS5-interacting network. A, Overlap of host proteins interacting with different orthoflaviviral NS5 proteins (ZIKV, USUV and WNV). BioVenn was used to the graphic representation of the diagram [99]. B, Gene Ontology analysis of cellular components (GO-CC). Related sub-compartments, i.e. mitochondrial inner membrane (GO:0005743) and mitochondrial nucleoid (GO:0042645) were grouped as 'Mitochondria' to reflect organelle-level localization. The pie chart displays the proportional distribution of significantly enriched terms (adjusted $p < 0.05$) among all factors identified in NS5-interacting datasets. C, Heatmap of significantly enriched Gene Ontology Biological Process (GO-BP) terms in co-IPs of cells transfected with either ZIKV, USUV, or WNV HA-tagged NS5 proteins (adjusted $p < 0.05$). Each GO-BP is represented in a colour-based gradient for statistical significance [$\sqrt{(-\log_{10}}$ adjusted p-value]. GO terms were clustered hierarchically using semantic similarity (rrvgo; similarity threshold = 0.7). See Supplementary Tables S5 and S6 for full terms.

Figure 2. Orthoflavivirus NS5 interaction network. Quantitative proteomics was used as described in the text to identify host factors interacting with HA-tagged versions of ZIKV, USUV or WNV NS5 proteins. Only the top 50 most significantly enriched factors in each data set are used to build the network and to identify overlaps between data sets. The protein-protein interaction network was generated using the STRING database [100]. Data clustering was generated in Cystoscape [101], using the MCL algorithm. Those factors identified in two datasets are coloured in pale yellow, and those in all three

datasets in coral. Each grey-shaded area represents a cluster positively associated with a biological process (i.e. ribosome biogenesis, cytoplasmic translation, mRNA processing, chromatin organisation, proton transmembrane transport/aerobic respiration). Mitochondrial proteins are encircled by a dashed line.

Figure 3. DsiRNA-mediated gene silencing identifies putative proviral and restriction host factors for OFV replication. Virus titres in the cellular supernatant of infected cells ($n \geq 4$ biologically independent samples), previously transfected with a DsiRNA targeting an NS5-interacting factor. At 24 h post-transfection, A549 cells were infected with either ZIKV (black columns) or USUV (grey columns) at an MOI of 0.1 $TCID_{50}$/cell. Control infections were carried out in parallel experiments in cells transfected with a non-human target DsiRNA (NonSP). Relative changes in viral titres observed at 48 h postinfection in gene-silenced cultures compared to NonSP controls are shown. For clarity, the effect of host factor downregulation on viral infectivity is represented in 3 different graphs: ribosome biogenesis and translation (A), mitochondrial (B), and other ungrouped host factors (C). Significant differences observed between unspecific (NonSP) and specific host-targeting DsiRNA-transfected cells are indicated (Two-way ANOVA, Dunnett's multiple comparisons test; *, $p < 0.05$; **, $p < 0.01$; ***, $p < 0.001$). Bars are representing the standard error of the mean (SEM) for each data point.

Figure 4. Reduced virus titres in MYOF-depleted cells. A – D, Effect of MYOF gene silencing on viral replication. A, Relative amount of metabolically active cells after transfection with a specific (DsiMYOF) or an unspecific DsiRNA (DsiNonSP). Cell viability is determined at 48 and 72 h post-transfection as suggested in the Methods section. Values are obtained as a percentage relative to mock untransfected cells. B, Relative MYOF mRNA expression was examined by RT-qPCR in A549 cells transfected with either

a MYOF-targeting (DsiMYOF) or a non-human target DsiRNA (DsiNonSP). MYOF mRNA levels were normalised to GAPDH mRNA levels. Values obtained are the average of at least 4 independent biological replicas (n ≥ 4), and relative to untransfected cells carried out in parallel. C, D, Virus infectivity was examined by $TCID_{50}$ assays of samples collected at different time points from cells previously transfected with each DsiRNA. Twenty-four hours after transfection, cells were infected with ZIKV (C) or USUV (D) at an MOI of 1 $TCID_{50}$/cell. Each value in the graph is the average of ≥ 4 independent biological replicas. E – G, Effect of MYOF-targeting drug WJ460 on ZIKV and USUV replication. E, The relative amount of metabolically active cells after treatment during 48 h with increasing concentrations of WJ460 is calculated as indicated in (A). Values are represented as a percentage relative to mock-treated cells. F, G, ZIKV (F) or USUV (G) titres detected in cells treated with WJ460 at 48 h postinfection. In each panel, significant differences are indicated (Two-way ANOVA, Sidak's multiple comparisons test; *, $p<0.05$; ***, $p < 0.001$). The standard error of the mean (SEM) is represented for each data point.

Figure 5. Increased viral titres, RNA and protein levels in PHB2-depleted cells. A, Relative PHB2 mRNA expression in A549 cells previously transfected with either a PHB2-targeting (DsiPHB2) or a non-human target DsiRNA (DsiNonSP). PHB2 expression was normalised to GAPDH mRNA levels. Values obtained are the average of at least 4 independent biological replicas (n ≥ 4), and relative to untransfected cells carried out in parallel. B, PHB2 downregulation leads to increased ZIKV NS5 protein abundance in infected cells. Representative WB of ZIKV NS5 and PHB2 protein levels in A549 cells previously transfected with each DsiRNA and infected at 24 h post-transfection with ZIKV. As a loading reference, an anti-GAPDH antibody was used. C – F, Virus infectivity was examined in the supernatants of cells previously transfected with each DsiRNA. Twenty-four hours after DsiRNA transfection, cells were infected with ZIKV (C, D) or USUV (E, F)

at an MOI of 0.1 (C, E) or 1 $TCID_{50}$/cell (D, F). Each value in the graph is the average of four independent biological replicas (n = 4). G – J, Viral RNA genome equivalents detected in samples collected at 48 h postinfection from cells previously transfected with each DsiRNA. Twenty-four hours after DsiRNA transfection, cells were infected at an MOI of 0.1 or 1 $TCID_{50}$/cell with ZIKV (G, H) or USUV (I, J). Each value in the graph represents the average of viral RNA detected in four independent biological replicas (n = 4) extracted from infected cells (intracellular, graphs G and I) or the supernatant of these cultures (graphs H and J). The statistical significance in each panel was determined by Two-way ANOVA and Sidak's multiple comparison test (C – J) or *t* (A) tests (*, $p<0.05$; **, $p<0.01$; ***, $p < 0.001$). Bars are representing the standard error of the mean (SEM).

Figure 6. Increased ZIKV titres and RNA levels in cells treated with a mitophagy inhibitor. A, Relative number of metabolically active A549 cells after 48 hours in the presence of increasing concentrations of mdivi-1. Values are relative to untreated cells (0 μM). B, ZIKV titres at 48 h post-infection in the supernatant of cells treated with increasing concentrations of mdivi-1. Cells were previously inoculated with ZIKV at an MOI of 0.1 $TCID_{50}$/cell. C, Genomic RNA equivalents in cells infected with ZIKV, and treated with mdivi-1. D, Relative IFNB1 mRNA expression in ZIKV-infected cells treated with mdivi-1.

Figure 7. PHB2 is transiently eliminated in ZIKV- and USUV-infected cells. (A, E) Representative blot of PHB2 kinetics in cells infected with either ZIKV (A) or USUV (E). B, C, F, G, PHB2 protein levels in mock- (B, F), ZIKV- (C) or USUV-infected (G) A549 cell lysates cells at different time points. PHB2 to tubulin band intensity ratios are relative to those obtained at 48 h in Mock-infected cultures. D, ZIKV NS5 protein levels detected in ZIKV-infected A549 cell lysates collected at different time points. NS5 to tubulin band intensity ratios for each time point are relative to 72 h post-infection. Each value in the

graphs is the average of three independent biological replicas (n = 3). Bars are representing the standard error of the mean (SEM) for each data point. Significant differences between mock and infected samples are indicated (One-way ANOVA; *, $p < 0.05$; **, $p < 0.01$). H, Representative blot of PHB2 protein levels in 293T cells collected at different time post-infection in cells infected with ZIKV (top) or USUV (bottom). An anti-GAPDH antibody was used to calibrate total protein loading.

Figure 8. Increased IFN-I transcription in PHB2-downregulated cells. A – D, Relative IFNB1 mRNA expression in A549 cells previously transfected with either a PHB2-targeting (DsiPHB2) or a non-human target (DsiNonSP) DsiRNA, and then infected with ZIKV (A, B) or USUV (C, D). IFNB1 expression was normalised to GAPDH mRNA levels. E – H, Relative IFNB1 mRNA expression in A549 cells transfected with either a PHB2-targeting (DsiPHB2) or a non-human target (DsiNonSP) DsiRNA, and then stimulated with different amounts of poly I:C. IFNB1 expression was normalised to GAPDH mRNA levels. Values obtained are the average of at least 4 independent biological replicas, and relative to control cells (no DsiRNA). E, G, IFNB1 mRNA levels in poly I:C-stimulated cells compared to control unstimulated cells. F, H, Relative IFNB1 mRNA expression in PHB2-depleted cells compared to control cells (DsiNonSP) after poly I:C stimulation.

Figure 9. Ectopic co-expression of NS2B3 and NS5 mediates efficient PHB2 elimination. A, B, PHB2 is co-immunoprecipitated with ZIKV, USUV and WNV NS5 proteins (A) or their RdRp domains (B). To this, 293T cells were transfected with constructs expressing HA-tagged versions of each NS5 (A), or the RdRp domain alone (B). As controls, there were included mock-transfected cells or constructs expressing EYFP (pEYFP-N1, shown as pEYFP), HA-tagged LacZ (pCruz HA-LacZ, shown as HA-LacZ) or an empty vector (pcDNA3). Cell lysates were incubated with anti-HA agarose (A,

B) or anti-EGFP (C) beads, and PHB2 co-immunoprecipitation together with NS5 and RdRp was examined, with a specific anti-PHB2 antibody. C, ZIKV NS5 overexpression leads to reduced STAT2 but not PHB2 levels. 293T cells were transfected with increasing amounts (400, 800, 1600, 3200 ng) of either a construct expressing an HA-tagged version of ZIKV NS5 or an empty vector (pcDNA3). D, Ectopic expression of NS2B/NS3 precursor (NS2B3) leads to reduced levels of PHB2 in 293T cells. To this, 5 x 10^5 293T cells were seeded on a 35-mm plate and transfected with either 2 or 4 μg of pZIKV-NS2B3 or an empty vector (pcDNA3). E, Enhanced PHB2 degradation in cells expressing both NS2B3 and NS5. In this assay, 5 x 10^5 293T cells were seeded on a 35-mm plate and co-transfected with 2 μg of pZIKV-NS2B3 and 2 μg of pZIKV-NS5 or an empty vector (pcDNA3). F, Increasing amounts of NS5 enhance PHB2 degradation in cells expressing a suboptimal amount of NS2B/NS3 protease. Transfections were carried out upon 5 x 10^6 293T cells previously seeded on 100-mm plates. Cells were lipofected with 2 μg of pZIKV-NS2B3 and different amounts of pZIKV-HA-NS5 (gradually increasing from 0.5 to 6 μg).

REFERENCES

1. Lim A, Shearer FM, Sewalk K, Pigott DM, Clarke J, Ghouse A, et al. The overlapping global distribution of dengue, chikungunya, Zika and yellow fever. Nat Commun. 2025;16: 3418. doi:10.1038/s41467-025-58609-5

2. Xu Y, Zhou J, Liu T, Liu P, Wu Y, Lai Z, et al. Assessing the risk of spread of Zika virus under current and future climate scenarios. Biosaf Health. 2022;4: 193–204. doi:10.1016/j.bsheal.2022.03.012

3. Malavige GN, Sjö P, Singh K, Piedagnel J-M, Mowbray C, Estani S, et al. Facing the escalating burden of dengue: Challenges and perspectives. PLOS Global Public Health. 2023;3: e0002598. doi:10.1371/journal.pgph.0002598

4. Pierson TC, Diamond MS. The continued threat of emerging flaviviruses. Nat Microbiol. 2020;5: 796–812. doi:10.1038/s41564-020-0714-0

5. de Souza WM, Weaver SC. Effects of climate change and human activities on vector-borne diseases. Nat Rev Microbiol. 2024;22: 476–491. doi:10.1038/s41579-024-01026-0

6. Roiz D, Pontifes PA, Jourdain F, Diagne C, Leroy B, Vaissière A-C, et al. The rising global economic costs of invasive Aedes mosquitoes and Aedes-borne diseases. Sci Total Environ. 2024;933: 173054. doi:10.1016/j.scitotenv.2024.173054

7. Moore SM, Oidtman RJ, James Soda K, Siraj AS, Reiner RC, Barker CM, et al. Leveraging multiple data types to estimate the size of the Zika epidemic in the Americas. PLoS Negl Trop Dis. 2020;14: e0008640. doi:10.1371/JOURNAL.PNTD.0008640

8. Cochet A, Calba C, Jourdain F, Grard G, Durand GA, Guinard A, et al. Autochthonous dengue in mainland France, 2022: geographical extension and incidence increase. Eurosurveillance. 2022;27: 1. doi:10.2807/1560-7917.ES.2022.27.44.2200818

9. Musso D, Ko AI, Baud D. Zika Virus Infection — After the Pandemic. New England Journal of Medicine. 2019;381: 1444–1457. doi:10.1056/nejmra1808246

10. Miner JJ, Diamond MS. Zika Virus Pathogenesis and Tissue Tropism. Cell Host Microbe. 2017;21: 134–142. doi:10.1016/j.chom.2017.01.004

11. Ferraris P, Yssel H, Missé D. Zika virus infection: an update. Microbes Infect. 2019;21: 353–360. doi:10.1016/j.micinf.2019.04.005

12. Santana LMB, de Moura IA, Mouzinho Ramos Tanaka Y, França RF de O. Zika Virus: A Review of Biology, Clinical Impacts, and Coinfections. Viruses. 2025;17: 637. doi:10.3390/v17050637

13. Scaramozzino P, Carvelli A, Bruni G, Cappiello G, Censi F, Magliano A, et al. West Nile and Usutu viruses co-circulation in central Italy: outcomes of the 2018 integrated surveillance. Parasit Vectors. 2021;14: 243. Available: https://parasitesandvectors.biomedcentral.com/articles/10.1186/s13071-021-04736-z

14. Brüssow H, Figuerola J. The Spread of the Mosquito-Transmitted West Nile Virus in North America and Europe. Microb Biotechnol. 2025;18. doi:10.1111/1751-7915.70120

15. Moir M, Sitharam N, Hofstra LM, Dor G, Mwanyika G, Ramphal Y, et al. Identifying genomic surveillance gaps in Africa for the global public health response to West Nile virus: a systematic review. Lancet Microbe. 2025;6: 101176. doi:10.1016/j.lanmic.2025.101176

16. Simonin Y. Un second cas autochtone d'infection par le virus Usutu détecté en France : que faut-il savoir ? In: The Conversation [Internet]. 2022 [cited 16 Jan 2023]. Available: https://theconversation.com/un-second-cas-autochtone-dinfection-par-le-virus-usutu-detecte-en-france-que-faut-il-savoir-97944

17. Clé M, Beck C, Salinas S, Lecollinet S, Gutierrez S, Van de Perre P, et al. Usutu virus: A new threat? Epidemiol Infect. 2019;147: e232. doi:10.1017/S0950268819001213

18. Simonin Y. Circulation of West Nile Virus and Usutu Virus in Europe: Overview and Challenges. Viruses. 2024;16: 599. doi:10.3390/v16040599

19. Cadar D, Maier P, Müller S, Kress J, Chudy M, Bialonski A, et al. Blood donor screening for West Nile virus (WNV) revealed acute Usutu virus (USUV) infection, Germany, September 2016. Eurosurveillance. 2017;22: 30501. doi:10.2807/1560-7917.ES.2017.22.14.30501

20. Bakonyi T, Jungbauer C, Aberle SW, Kolodziejek J, Dimmel K, Stiasny K, et al. Usutu virus infections among blood donors, Austria, July and August 2017 – Raising awareness for diagnostic challenges. Eurosurveillance. 2017;22. doi:10.2807/1560-7917.ES.2017.22.41.17-00644

21. Madere FS, Andrade da Silva AV, Okeze E, Tilley E, Grinev A, Konduru K, et al. Flavivirus infections and diagnostic challenges for dengue, West Nile and Zika Viruses. npj Viruses. 2025;3: 36. doi:10.1038/s44298-025-00114-z

22. Wahaab A, Mustafa BE, Hameed M, Stevenson NJ, Anwar MN, Liu K, et al. Potential Role of Flavivirus NS2B-NS3 Proteases in Viral Pathogenesis and Anti-flavivirus Drug Discovery Employing Animal Cells and Models: A Review. Viruses. 2021;14: 44. doi:10.3390/v14010044

23. Ferrero DS, Ruiz-Arroyo VM, Soler N, Usón I, Guarné A, Verdaguer N. Supramolecular arrangement of the full-length Zika virus NS5. Rey FA, editor. PLoS Pathog. 2019;15: e1007656. doi:10.1371/journal.ppat.1007656

24. Denolly S, Stukalov A, Barayeu U, Rosinski AN, Kritsiligkou P, Joecks S, et al. Zika virus remodelled ER membranes contain proviral factors involved in redox and methylation pathways. Nat Commun. 2023;14: 8045. doi:10.1038/s41467-023-43665-6

25. Welsch S, Miller S, Romero-Brey I, Merz A, Bleck CKE, Walther P, et al. Composition and three-dimensional architecture of the dengue virus replication and assembly sites. Cell Host Microbe. 2009;5: 365–75. doi:10.1016/j.chom.2009.03.007

26. Ci Y, Shi L. Compartmentalized replication organelle of flavivirus at the ER and the factors involved. Cellular and Molecular Life Sciences 2021 78:11. 2021;78: 4939–4954. doi:10.1007/S00018-021-03834-6

27. Scaturro P, Stukalov A, Haas DA, Cortese M, Draganova K, Płaszczyca A, et al. An orthogonal proteomic survey uncovers novel Zika virus host factors. Nature. 2018;561: 253–257. doi:10.1038/s41586-018-0484-5

28. Schneider WM, Hoffmann HH. Flavivirus-host interactions: an expanding network of proviral and antiviral factors. Curr Opin Virol. 2022;52: 71–77. doi:10.1016/J.COVIRO.2021.11.007

29. Li P, Wu J, Liu S, Lu R, Jiang H, Wang N, et al. The RNA polymerase of cytoplasmically replicating Zika virus binds with chromatin DNA in nuclei and regulates host gene transcription. Proceedings of the National Academy of Sciences. 2022;119. doi:10.1073/pnas.2205013119

30. Lebeau G, Hoareau M, Rivière S, El Safadi D, Da Silva CR, Krejbich-Trotot P, et al. Cell cycle and mitosis progression during ZIKA virus infection: The viral non-structural protein NS5 as a master regulator of the APC/cyclosome? Biochimie. 2024;221: 75–80. doi:10.1016/j.biochi.2024.01.016

31. Best SM. The Many Faces of the Flavivirus NS5 Protein in Antagonism of Type I Interferon Signaling. J Virol. 2017;91. doi:10.1128/JVI.01970-16

32. Albentosa-González L, Jimenez de Oya N, Arias A, Clemente-Casares P, Martin-Acebes MÁ, Saiz JC, et al. Akt Kinase Intervenes in Flavivirus Replication by Interacting with Viral Protein NS5. Viruses. 2021;13: 896. Available: http://www.ncbi.nlm.nih.gov/pubmed/34066055

33. Rodrigo I, Albentosa-González L, Romero de Ávila MJ, Bassi MR, Sempere RN, Clemente-Casares P, et al. Ubiquitin-like modifier-activating enzyme 1 interacts with Zika virus NS5 and promotes viral replication in the infected cell. J Gen Virol. 2025;106: 002063. doi:10.1099/jgv.0.002063

34. Saade M, Ferrero DS, Blanco-Ameijeiras J, Gonzalez-Gobartt E, Flores-Mendez M, Ruiz-Arroyo VM, et al. Multimerization of Zika Virus-NS5 Causes Ciliopathy and Forces Premature Neurogenesis. Cell Stem Cell. 2020;27: 920-936.e8. doi:10.1016/j.stem.2020.10.002

35. Deb A, Nagpal S, Yadav RK, Thakur H, Nair D, Krishnan V, et al. Japanese encephalitis virus NS5 protein interacts with nucleolin to enhance the virus replication. J Virol. 2024;98. doi:10.1128/jvi.00858-24

36. Grant A, Ponia SS, Tripathi S, Balasubramaniam V, Miorin L, Sourisseau M, et al. Zika Virus Targets Human STAT2 to Inhibit Type i Interferon Signaling. Cell Host Microbe. 2016;19: 882–890. doi:10.1016/j.chom.2016.05.009

37. Gonzalez Lopez Ledesma MM, Costa Navarro G, Pallares HM, Paletta A, De Maio F, Iglesias NG, et al. Dengue virus NS5 degrades ERC1 during infection to antagonize NF-kB activation. Proceedings of the National Academy of Sciences. 2023;120. doi:10.1073/pnas.2220005120

38. Ren W, Fu C, Zhang Y, Ju X, Jiang X, Song J, et al. Zika virus NS5 protein inhibits type I interferon signaling via CRL3 E3 ubiquitin ligase-mediated degradation of STAT2. Proc Natl Acad Sci U S A. 2024;121: e2403235121. doi:10.1073/pnas.2403235121

39. Liu Y, Zhou T, Hu J, Jin S, Wu J, Guan X, et al. Targeting Selective Autophagy as a Therapeutic Strategy for Viral Infectious Diseases. Front Microbiol. 2022;13. doi:10.3389/fmicb.2022.889835

40. Yan C, Gong L, Chen L, Xu M, Abou-Hamdan H, Tang M, et al. PHB2 (prohibitin 2) promotes PINK1-PRKN/Parkin-dependent mitophagy by the PARL-PGAM5-PINK1 axis. Autophagy. 2020;16: 419–434. doi:10.1080/15548627.2019.1628520

41. Jin SM, Youle RJ. PINK1- and Parkin-mediated mitophagy at a glance. J Cell Sci. 2012;125: 795–799. doi:10.1242/jcs.093849

42. Dagda RK, Cherra SJ, Kulich SM, Tandon A, Park D, Chu CT. Loss of PINK1 Function Promotes Mitophagy through Effects on Oxidative Stress and Mitochondrial Fission. Journal of Biological Chemistry. 2009;284: 13843–13855. doi:10.1074/jbc.M808515200

43. Cheng M, Lin N, Dong D, Ma J, Su J, Sun L. PGAM5: A crucial role in mitochondrial dynamics and programmed cell death. Eur J Cell Biol. 2021;100: 151144. Available: https://linkinghub.elsevier.com/retrieve/pii/S0171933520300832

44. Xiao Y, Zhou Y, Lu Y, Zhou K, Cai W. PHB2 interacts with LC3 and SQSTM1 is required for bile acids-induced mitophagy in cholestatic liver. Cell Death Dis. 2018;9: 160. doi:10.1038/s41419-017-0228-8

45. Boytz R, Keita K, Pawlak JB, Laurent-Rolle M. Flaviviruses manipulate mitochondrial processes to evade the innate immune response. npj Viruses. 2024;2: 47. doi:10.1038/s44298-024-00057-x

46. Agarwal A, Alam MF, Basu B, Pattanayak S, Asthana S, Syed GH, et al. Japanese Encephalitis Virus NS4A Protein Interacts with PTEN-Induced Kinase 1 (PINK1) and Promotes Mitophagy in Infected Cells. Ramage H, editor. Microbiol Spectr. 2022;10: e0083022. Available: http://www.ncbi.nlm.nih.gov/pubmed/35604158

47. Khan M, Syed GH, Kim SJ, Siddiqui A. Mitochondrial dynamics and viral infections: A close nexus. Biochim Biophys Acta. 2015;1853: 2822–2833. doi:10.1016/J.BBAMCR.2014.12.040

48. Singh B, Avula K, Sufi SA, Parwin N, Das S, Alam MF, et al. Defective Mitochondrial Quality Control during Dengue Infection Contributes to Disease Pathogenesis. Ou J-HJ, editor. J Virol. 2022;96: e0082822. Available: http://www.ncbi.nlm.nih.gov/pubmed/36197108

49. Ponia SS, Robertson SJ, McNally KL, Subramanian G, Sturdevant GL, Lewis M, et al. Mitophagy antagonism by ZIKV reveals Ajuba as a regulator of PINK1 signaling, PKR-dependent inflammation, and viral invasion of tissues. Cell Rep. 2021;37: 109888. Available: https://linkinghub.elsevier.com/retrieve/pii/S2211124721013589

50. Lee JK, Shin OS. Zika virus modulates mitochondrial dynamics, mitophagy, and mitochondria-derived vesicles to facilitate viral replication in trophoblast cells. Front Immunol. 2023;14. doi:10.3389/fimmu.2023.1203645

51. Bassi MR, Sempere RN, Meyn P, Polacek C, Arias A. Extinction of Zika virus and Usutu virus by lethal mutagenesis reveals different patterns of sensitivity to three mutagenic drugs. Antimicrob Agents Chemother. 2018;62: e00380-18. doi:10.1128/AAC.00380-18

52. Sempere RN, Arias A. Establishment of a Cell Culture Model of Persistent Flaviviral Infection: Usutu Virus Shows Sustained Replication during Passages and Resistance to Extinction by Antiviral Nucleosides. Viruses. 2019;11: 560. Available: https://www.mdpi.com/1999-4915/11/6/560

53. Martínez-González B, Gallego I, Gregori J, Soria ME, Somovilla P, de Ávila AI, et al. Fitness-Dependent, Mild Mutagenic Activity of Sofosbuvir for Hepatitis C Virus. Antimicrob Agents Chemother. 2023;67. doi:10.1128/aac.00394-23

54. Rodrigo I, Ballesta C, Nunes EB, Pérez P, García-Arriaza J, Arias A. Eeyarestatin I, an inhibitor of the valosin-containing protein, exhibits potent virucidal activity against the flaviviruses. Antiviral Res. 2022;207: 105416. doi:10.1016/J.ANTIVIRAL.2022.105416

55. Lindenbach BD. Measuring HCV Infectivity Produced in Cell Culture and In Vivo. Methods in molecular biology (Clifton, NJ). 2009. pp. 329–336. doi:10.1007/978-1-59745-394-3_24

56. Reed LJ, Muench H. A simple method of estimating fifty per cent endpoints. Am J Epidemiol. 1938;27: 493–497. doi:10.1093/oxfordjournals.aje.a118408

57. Livak KJ, Schmittgen TD. Analysis of relative gene expression data using real-time quantitative PCR and the 2-ΔΔCT method. Methods. 2001;25: 402–408. doi:10.1006/meth.2001.1262

58. Albentosa-González L, Sabariegos R, Arias A, Clemente-Casares P, Mas A. Akt interacts with usutu virus polymerase, and its activity modulates viral replication. Pathogens. 2021;10: 1–15.

59. Hughes CS, Moggridge S, Müller T, Sorensen PH, Morin GB, Krijgsveld J. Single-pot, solid-phase-enhanced sample preparation for proteomics experiments. Nat Protoc. 2019;14: 68–85. doi:10.1038/s41596-018-0082-x

60. Meyer B, Chiaravalli J, Gellenoncourt S, Brownridge P, Bryne DP, Daly LA, et al. Characterising proteolysis during SARS-CoV-2 infection identifies viral cleavage sites and cellular targets with therapeutic potential. Nature Communications 2021 12:1. 2021;12: 1–16. doi:10.1038/s41467-021-25796-w

61. Cox J, Mann M. MaxQuant enables high peptide identification rates, individualized p.p.b.-range mass accuracies and proteome-wide protein quantification. Nat Biotechnol. 2008;26: 1367–1372. doi:10.1038/nbt.1511

62. Nguyen SK, Anders N, Holmes S, Barrow HG, Lukhovitskaya N, Jahun AS, et al. Encephalomyocarditis virus protein 2B* interacts with 14-3-3 proteins through a phosphorylated C-terminal binding motif. mBio. 2025;16. doi:10.1128/mbio.01008-25

63. Zhang T, Li J, He Y, Yang F, Hao Y, Jin W, et al. A small molecule targeting myoferlin exerts promising anti-tumor effects on breast cancer. Nat Commun. 2018;9: 3726. doi:10.1038/s41467-018-06179-0

64. Bordt EA, Clerc P, Roelofs BA, Saladino AJ, Tretter L, Adam-Vizi V, et al. The Putative Drp1 Inhibitor mdivi-1 Is a Reversible Mitochondrial Complex I Inhibitor that Modulates Reactive Oxygen Species. Dev Cell. 2017;40: 583-594.e6. doi:10.1016/j.devcel.2017.02.020

65. Yoshinaka T, Kosako H, Yoshizumi T, Furukawa R, Hirano Y, Kuge O, et al. Structural Basis of Mitochondrial Scaffolds by Prohibitin Complexes: Insight into a Role of the Coiled-Coil Region. iScience. 2019;19: 1065. doi:10.1016/J.ISCI.2019.08.056

66. Zhou P, Zhang Q, Yang Y, Wu W, Chen D, Zheng Z, et al. Cleavage of SQSTM1/p62 by the Zika virus protease NS2B3 prevents autophagic degradation of viral NS3 and NS5 proteins. Autophagy. 2024;20: 2769–2784. doi:10.1080/15548627.2024.2390810

67. Ding Q, Gaska JM, Douam F, Wei L, Kim D, Balev M, et al. Species-specific disruption of STING-dependent antiviral cellular defenses by the Zika virus NS2B3 protease. Proceedings of the National Academy of Sciences. 2018;115. doi:10.1073/pnas.1803406115

68. Lennemann NJ, Coyne CB. Dengue and Zika viruses subvert reticulophagy by NS2B3-mediated cleavage of FAM134B. Autophagy. 2017;13: 322–332. doi:10.1080/15548627.2016.1265192

69. Wang L, Zhang X, Huang X, Sha X, Li X, Zheng J, et al. Homoplantaginin alleviates high glucose-induced vascular endothelial senescence by inhibiting mtDNA–cGAS–STING pathway via blunting DRP1–mitochondrial fission–VDAC1 axis. The FASEB Journal. 2024;38. doi:10.1096/fj.202401299RR

70. Qi Y, Rajbanshi B, Hao R, Dang Y, Xu C, Lu W, et al. The dual role of PGAM5 in inflammation. Exp Mol Med. 2025;57: 298–311. doi:10.1038/s12276-025-01391-7

71. Bavelloni A, Piazzi M, Raffini M, Faenza I, Blalock WL. Prohibitin 2: At a communications crossroads. IUBMB Life. 2015;67: 239–254. doi:10.1002/iub.1366

72. Sun L, Liu L, Yang X-J, Wu Z. Akt binds prohibitin 2 and relieves its repression of MyoD and muscle differentiation. J Cell Sci. 2004;117: 3021–3029. doi:10.1242/jcs.01142

73. Ding T, Xu H, Zhang X, Yang F, Zhang J, Shi Y, et al. Prohibitin 2 orchestrates long noncoding RNA and gene transcription to accelerate tumorigenesis. Nat Commun. 2024;15: 8385. doi:10.1038/s41467-024-52425-z

74. Kasashima K, Ohta E, Kagawa Y, Endo H. Mitochondrial Functions and Estrogen Receptor-dependent Nuclear Translocation of Pleiotropic Human Prohibitin 2. Journal of Biological Chemistry. 2006;281: 36401–36410. doi:10.1074/jbc.M605260200

75. Kim J, Akiyama M, Park J, Lin M, Shimo A, Ueki T, et al. Activation of an estrogen/estrogen receptor signaling by BIG3 through its inhibitory effect on nuclear transport of PHB2/REA in breast cancer. Cancer Sci. 2009;100: 1468–1478. doi:10.1111/j.1349-7006.2009.01209.x

76. Grady SF, Pinto AK, Hassert M, D'Angelo JA, Brien JD, Arnatt CK. Selective estrogen receptor modulator, tamoxifen, inhibits Zika virus infection. J Med Virol. 2021;93: 6155–6162. doi:10.1002/JMV.27230

77. Oyang L, Li J, Jiang X, Lin J, Xia L, Yang L, et al. The function of prohibitins in mitochondria and the clinical potentials. Cancer Cell Int. 2022;22: 343. Available: https://cancerci.biomedcentral.com/articles/10.1186/s12935-022-02765-x

78. Eyre NS, Kirby EN, Anfiteatro DR, Bracho G, Russo AG, White PA, et al. Identification of Estrogen Receptor Modulators as Inhibitors of Flavivirus Infection. Antimicrob Agents Chemother. 2020;64: e00289-20. Available: https://journals.asm.org/doi/10.1128/AAC.00289-20

79. Celegato M, Sturlese M, Vasconcelos Costa V, Trevisan M, Lallo Dias AS, Souza Passos IB, et al. Small-Molecule Inhibitor of Flaviviral NS3-NS5 Interaction with Broad-Spectrum Activity and Efficacy *In Vivo*. mBio. 2023;14. doi:10.1128/mbio.03097-22

80. Tay MYF, Saw WG, Zhao Y, Chan KWK, Singh D, Chong Y, et al. The C-terminal 50 Amino Acid Residues of Dengue NS3 Protein Are Important for NS3-NS5 Interaction and Viral Replication. Journal of Biological Chemistry. 2015;290: 2379–2394. doi:10.1074/jbc.M114.607341

81. Zoladek J, Nisole S. Mosquito-borne flaviviruses and type I interferon: catch me if you can! Front Microbiol. 2023;14. doi:10.3389/fmicb.2023.1257024

82. Goh JZH, De Hayr L, Khromykh AA, Slonchak A. The Flavivirus Non-Structural Protein 5 (NS5): Structure, Functions, and Targeting for Development of Vaccines and Therapeutics. Vaccines (Basel). 2024;12: 865. doi:10.3390/vaccines12080865

83. Rehwinkel J, Gack MU. RIG-I-like receptors: their regulation and roles in RNA sensing. Nat Rev Immunol. 2020;20: 537–551. doi:10.1038/S41577-020-0288-3

84. Pan Y, Cai W, Cheng A, Wang M, Yin Z, Jia R. Flaviviruses: Innate Immunity, Inflammasome Activation, Inflammatory Cell Death, and Cytokines. Front Immunol. 2022;13: 829433. doi:10.3389/fimmu.2022.829433

85. Jiménez-Loygorri JI, Villarejo-Zori B, Viedma-Poyatos Á, Zapata-Muñoz J, Benítez-Fernández R, Frutos-Lisón MD, et al. Mitophagy curtails cytosolic mtDNA-dependent activation of cGAS/STING inflammation during aging. Nat Commun. 2024;15: 830. doi:10.1038/s41467-024-45044-1

86. Yuk J-M, Silwal P, Jo E-K. Inflammasome and Mitophagy Connection in Health and Disease. Int J Mol Sci. 2020;21: 4714. doi:10.3390/ijms21134714

87. Fu C, Cao N, Liu W, Zhang Z, Yang Z, Zhu W, et al. Crosstalk between mitophagy and innate immunity in viral infection. Front Microbiol. 2022;13. doi:10.3389/fmicb.2022.1064045

88. Wang S, Long H, Hou L, Feng B, Ma Z, Wu Y, et al. The mitophagy pathway and its implications in human diseases. Signal Transduct Target Ther. 2023;8: 304. doi:10.1038/s41392-023-01503-7

89. Gkikas I, Palikaras K, Tavernarakis N. The Role of Mitophagy in Innate Immunity. Front Immunol. 2018;9: 1283. doi:10.3389/FIMMU.2018.01283

90. Jin Y, Zhao L, Wang S, Zhang X, Quan J, Lin Z, et al. *RSL1D1* knockdown induces ferroptosis and mediates ferrous iron accumulation in senescent cells by inhibiting *FTH1* mRNA stability. Carcinogenesis. 2023;44: 129–142. doi:10.1093/carcin/bgad012

91. Liu X, Chen J, Long X, Lan J, Liu X, Zhou M, et al. RSL1D1 promotes the progression of colorectal cancer through RAN-mediated autophagy suppression. Cell Death Dis. 2022;13: 43. doi:10.1038/s41419-021-04492-z

92. Gupta S, Yano J, Mercier V, Htwe HH, Shin HR, Rademaker G, et al. Lysosomal retargeting of Myoferlin mitigates membrane stress to enable pancreatic cancer growth. Nat Cell Biol. 2021;23: 232–242. doi:10.1038/s41556-021-00644-7

93. Bernatchez PN, Sharma A, Kodaman P, Sessa WC. Myoferlin is critical for endocytosis in endothelial cells. American Journal of Physiology-Cell Physiology. 2009;297: C484–C492. doi:10.1152/ajpcell.00498.2008

94. Morita E, Suzuki Y. Membrane-Associated Flavivirus Replication Complex—Its Organization and Regulation. Viruses. 2021;13: 1060. doi:10.3390/v13061060

95. Cretu C, Chernev A, Kibédi Szabó CZ, Pena V, Urlaub H, Moser T, et al. Structural insights into lipid membrane binding by human ferlins. EMBO J. 2025. doi:10.1038/s44318-025-00463-8

96. He Y, Kan W, Li Y, Hao Y, Huang A, Gu H, et al. A potent and selective small molecule inhibitor of myoferlin attenuates colorectal cancer progression. Clin Transl Med. 2021;11. doi:10.1002/ctm2.289

97. Xu G, Xia Z, Deng F, Liu L, Wang Q, Yu Y, et al. Inducible LGALS3BP/90K activates antiviral innate immune responses by targeting TRAF6 and TRAF3 complex. PLoS Pathog. 2019;15: e1008002. doi:10.1371/journal.ppat.1008002

98. Arutyunov A, Durán-Laforet V, Ai S, Ferrari L, Murphy R, Schafer DP, et al. West Nile Virus-Induced Expression of Senescent Gene Lgals3bp Regulates Microglial Phenotype within Cerebral Cortex. Biomolecules. 2024;14: 808. doi:10.3390/biom14070808

99. Hulsen T, de Vlieg J, Alkema W. BioVenn – a web application for the comparison and visualization of biological lists using area-proportional Venn diagrams. BMC Genomics. 2008;9: 488. doi:10.1186/1471-2164-9-488

100. Szklarczyk D, Kirsch R, Koutrouli M, Nastou K, Mehryary F, Hachilif R, et al. The STRING database in 2023: protein–protein association networks and functional enrichment analyses for any sequenced genome of interest. Nucleic Acids Res. 2023;51: D638–D646. doi:10.1093/nar/gkac1000

101. Shannon P, Markiel A, Ozier O, Baliga NS, Wang JT, Ramage D, et al. Cytoscape: A Software Environment for Integrated Models of Biomolecular Interaction Networks. Genome Res. 2003;13: 2498–2504. doi:10.1101/gr.1239303

Figure 1

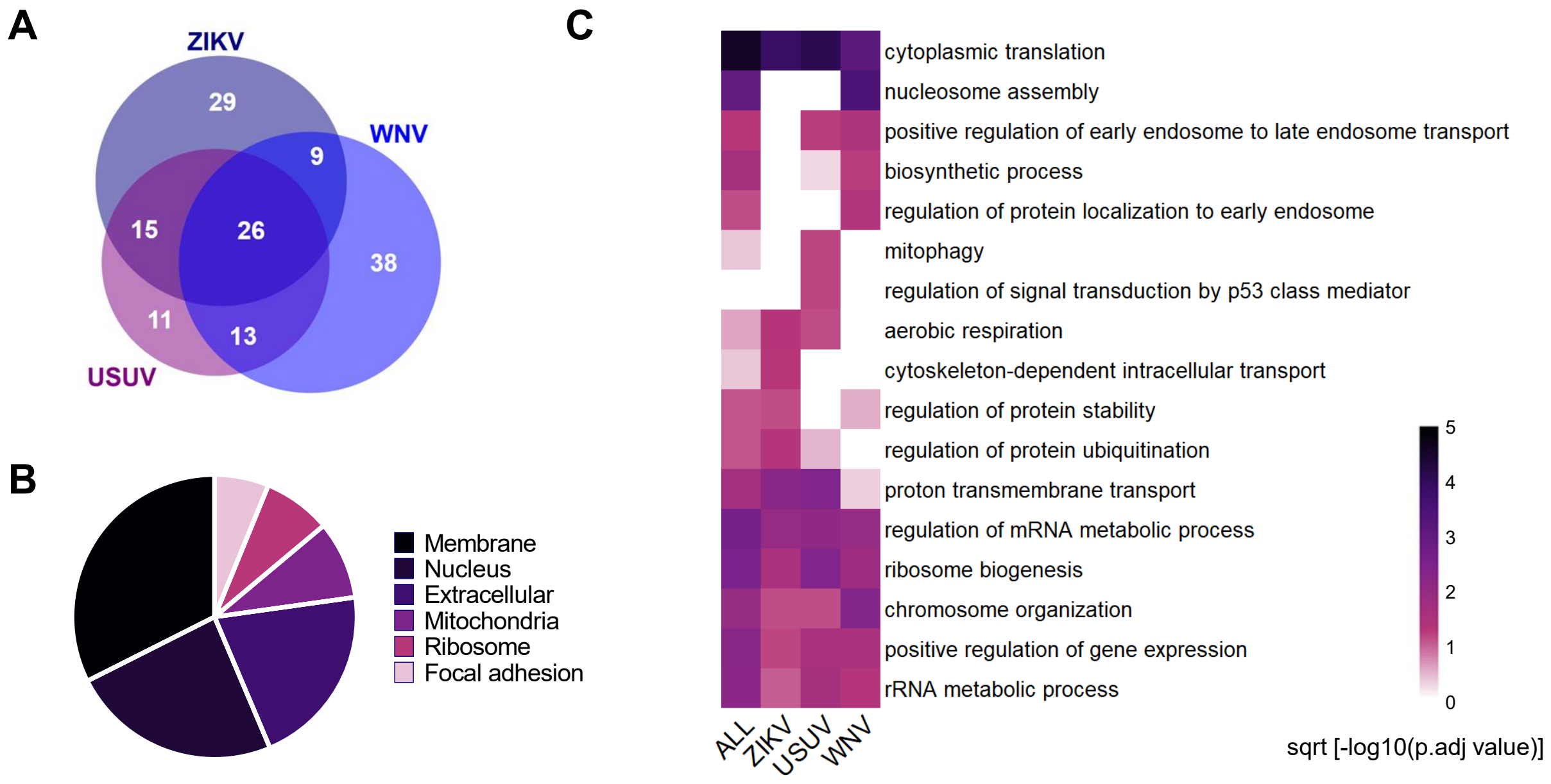
A
ZIKV
WNV
USUV
29
9
15
26
38
11
13
B
Membrane
Nucleus
Extracellular
Mitochondria
Ribosome
Focal adhesion
C
cytoplasmic translation
nucleosome assembly
positive regulation of early endosome to late endosome transport
biosynthetic process
regulation of protein localization to early endosome
mitophagy
regulation of signal transduction by p53 class mediator
aerobic respiration
cytoskeleton-dependent intracellular transport
regulation of protein stability
regulation of protein ubiquitination
proton transmembrane transport
regulation of mRNA metabolic process
ribosome biogenesis
chromosome organization
positive regulation of gene expression
rRNA metabolic process
ALL
ZIKV
USUV
WNV
5
4
3
2
1
0
sqrt [-log10(p.adj value)]

Figure 2

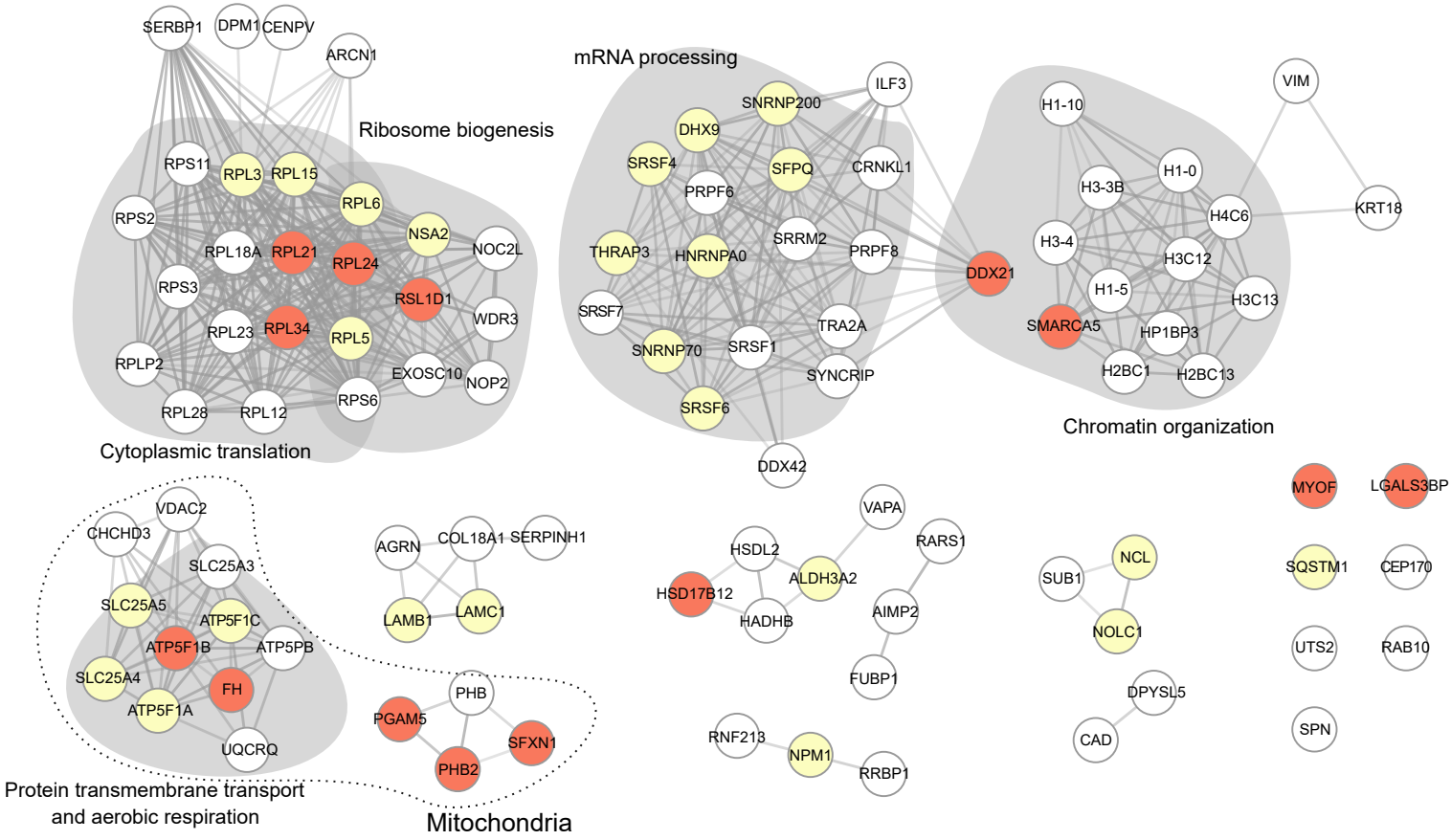
SERBP1
DPM1
CENPV
ARCN1
Ribosome biogenesis
RPS11
RPL3
RPL15
RPL6
RPS2
NSA2
NOC2L
RPL18A
RPL21
RPL24
RPS3
RSL1D1
WDR3
RPL23
RPL34
RPL5
RPLP2
EXOSC10
NOP2
RPS6
RPL28
RPL12
Cytoplasmic translation
mRNA processing
ILF3
SNRNP200
DHX9
SRSF4
SFPQ
CRNKL1
PRPF6
SRRM2
THRAP3
HNRNPA0
PRPF8
SRSF7
TRA2A
SNRNP70
SRSF1
SYNCRIP
SRSF6
DDX42
DDX21
VIM
H1-10
H1-0
H3-3B
H4C6
KRT18
H3-4
H3C12
H1-5
H3C13
SMARCA5
HP1BP3
H2BC1
H2BC13
Chromatin organization
VDAC2
CHCHD3
SLC25A3
SLC25A5
ATP5F1C
ATP5F1B
ATP5PB
SLC25A4
FH
ATP5F1A
UQCRQ
Protein transmembrane transport
and aerobic respiration
AGRN
COL18A1
SERPINH1
LAMB1
LAMC1
PHB
PGAM5
SFXN1
PHB2
Mitochondria
VAPA
HSDL2
RARS1
ALDH3A2
HSD17B12
AIMP2
HADHB
FUBP1
RNF213
NPM1
RRBP1
SUB1
NCL
NOLC1
DPYSL5
CAD
MYOF
LGALS3BP
SQSTM1
CEP170
UTS2
RAB10
SPN

Figure 3

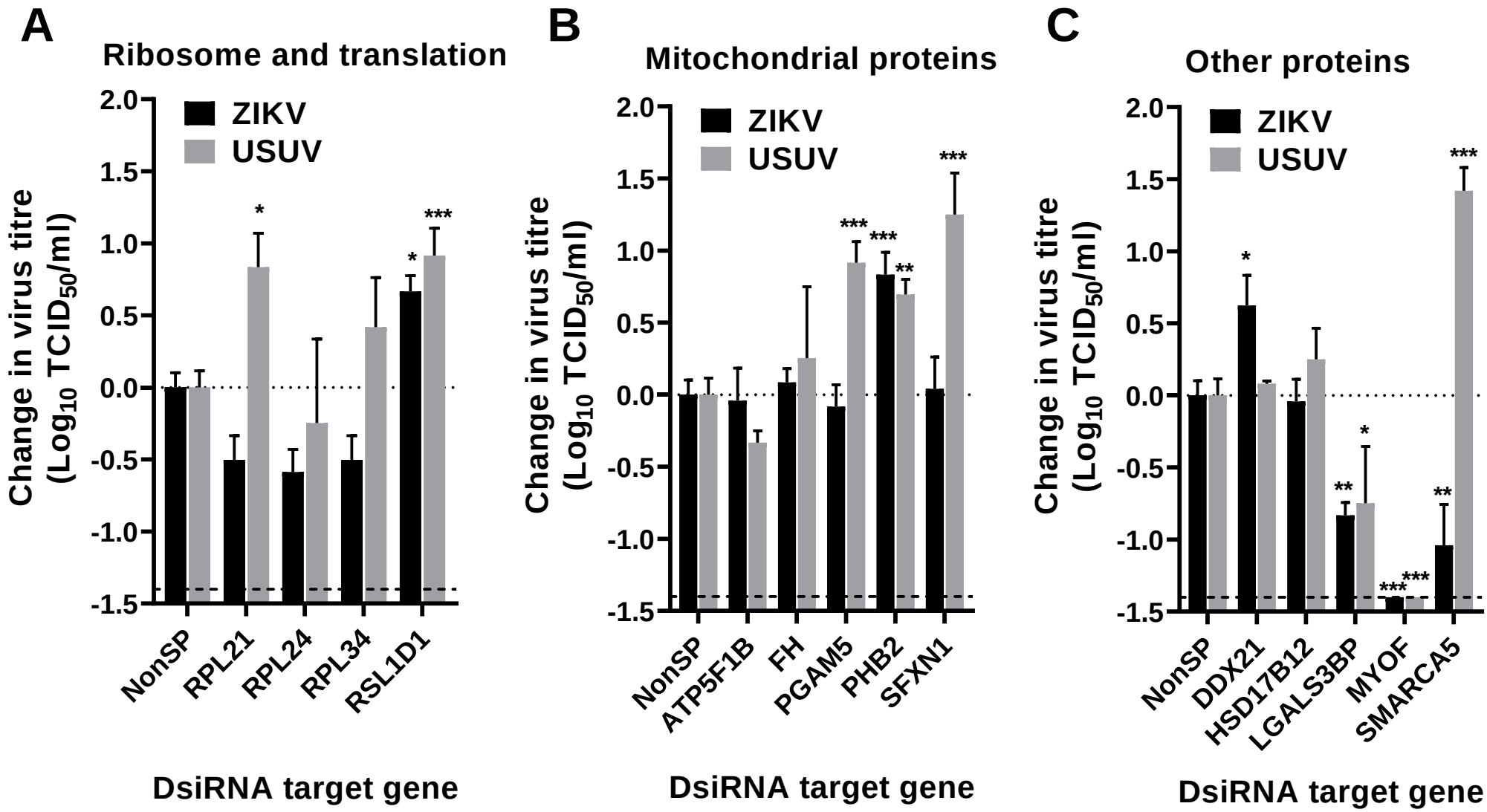
A
Ribosome and translation
ZIKV
USUV
Change in virus titre
(Log10 TCID50/ml)
2.0
1.5
1.0
0.5
0.0
-0.5
-1.0
-1.5
*
*
***
NonSP
RPL21
RPL24
RPL34
RSL1D1
DsiRNA target gene
B
Mitochondrial proteins
ZIKV
USUV
Change in virus titre
(Log10 TCID50/ml)
***
***
**
***
NonSP
ATP5F1B
FH
PGAM5
PHB2
SFXN1
DsiRNA target gene
C
Other proteins
ZIKV
USUV
Change in virus titre
(Log10 TCID50/ml)
*
**
*
***
***
**
***
NonSP
DDX21
HSD17B12
LGALS3BP
MYOF
SMARCA5
DsiRNA target gene

Figure 4

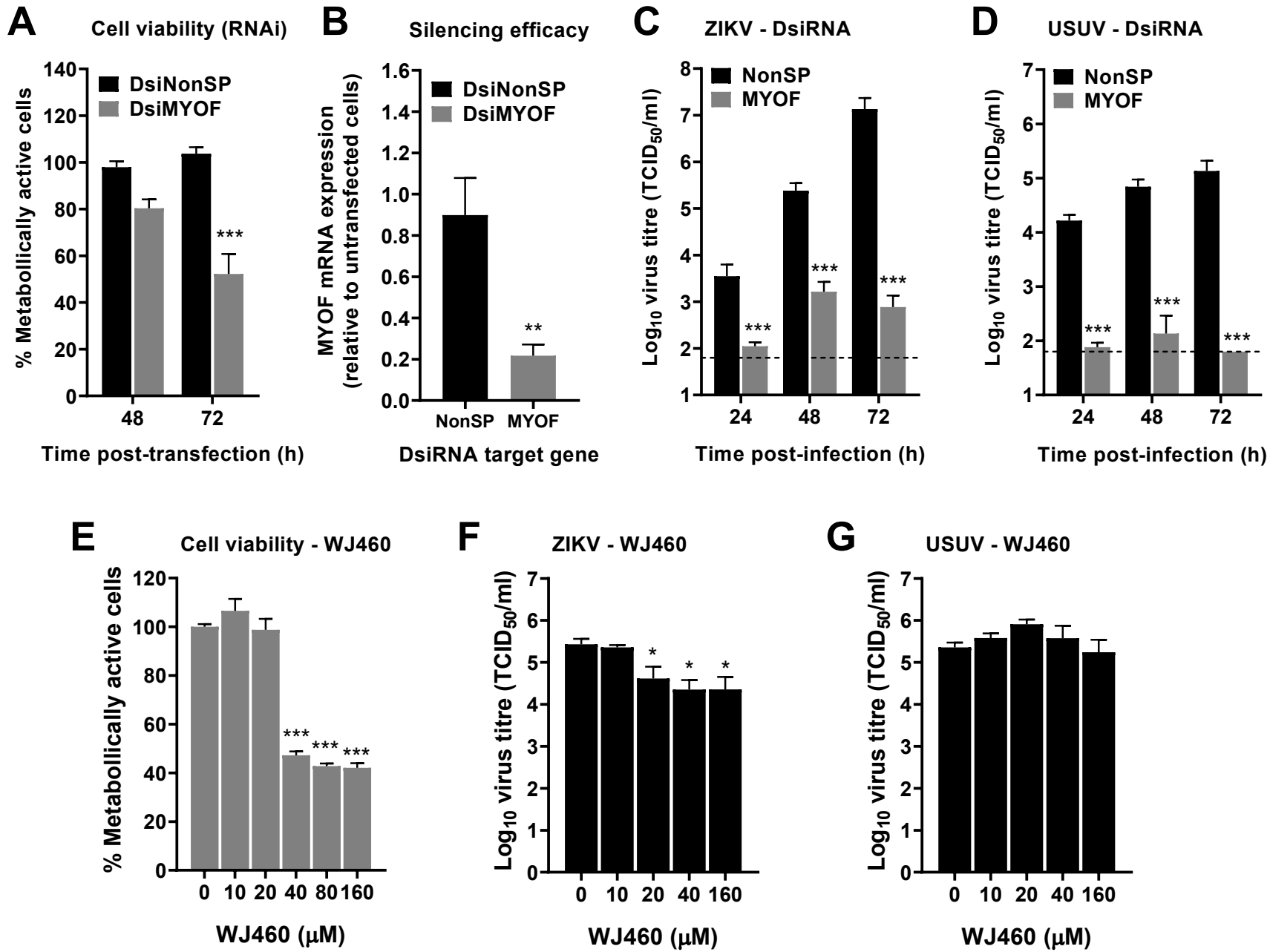
A
Cell viability (RNAi)
DsiNonSP
DsiMYOF
% Metabollically active cells
140
120
100
80
60
40
20
0
***
48
72
Time post-transfection (h)
B
Silencing efficacy
DsiNonSP
DsiMYOF
MYOF mRNA expression
(relative to untransfected cells)
1.6
1.4
1.2
1.0
0.8
0.6
0.4
0.2
0.0
**
NonSP
MYOF
DsiRNA target gene
C
ZIKV - DsiRNA
NonSP
MYOF
Log10 virus titre (TCID50/ml)
8
7
6
5
4
3
2
1
***
24
48
72
Time post-infection (h)
D
USUV - DsiRNA
NonSP
MYOF
Log10 virus titre (TCID50/ml)
7
6
5
4
3
2
1
***
24
48
72
Time post-infection (h)
E
Cell viability - WJ460
% Metabollically active cells
120
100
80
60
40
20
0
***
0 10 20 40 80 160
WJ460 (µM)
F
ZIKV - WJ460
Log10 virus titre (TCID50/ml)
7
6
5
4
3
2
1
0
*
0 10 20 40 160
WJ460 (µM)
G
USUV - WJ460
Log10 virus titre (TCID50/ml)
7
6
5
4
3
2
1
0
0 10 20 40 160
WJ460 (µM)

Figure 5

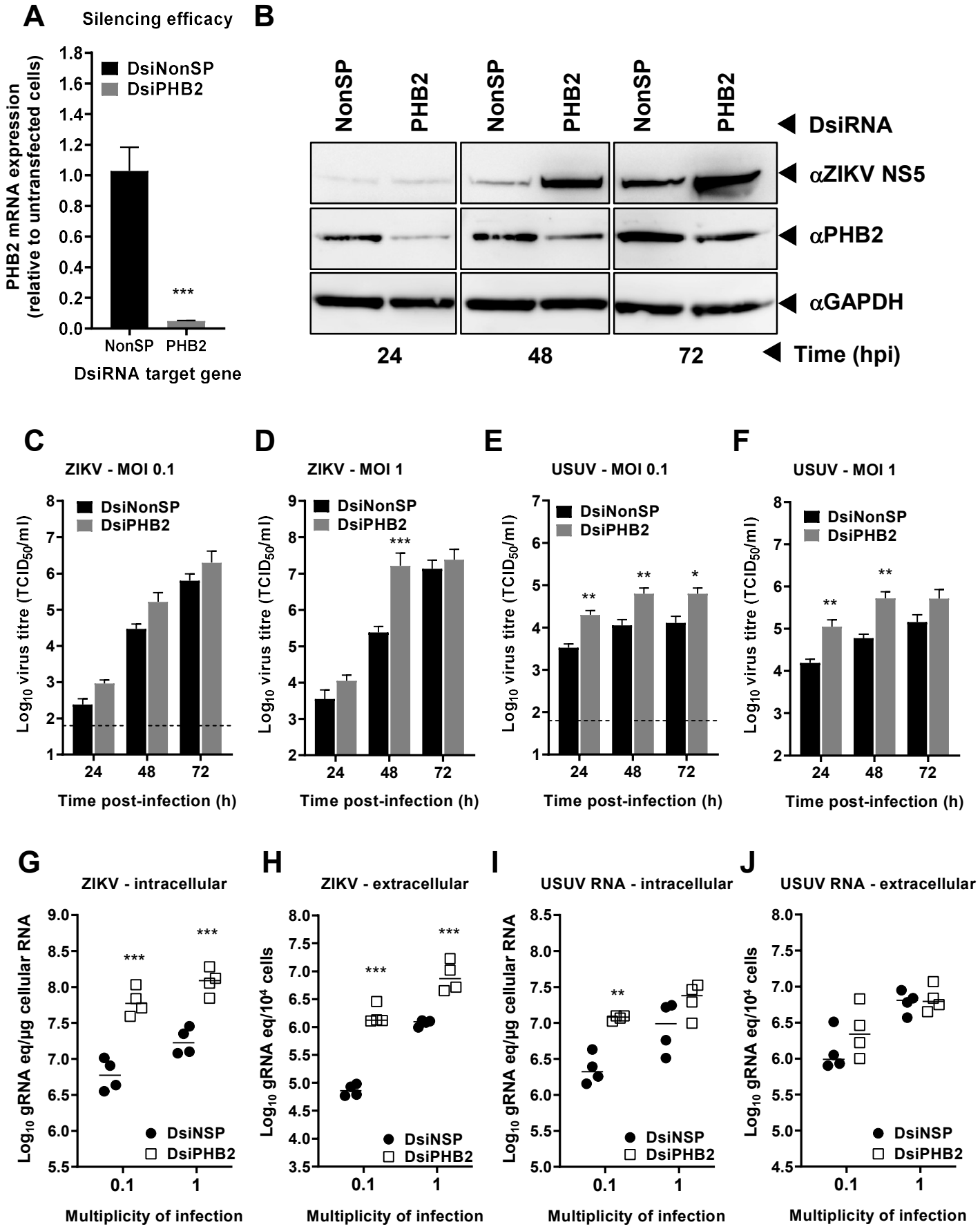
A
Silencing efficacy
PHB2 mRNA expression (relative to untransfected cells)
DsiNonSP
DsiPHB2
***
NonSP
PHB2
DsiRNA target gene
B
NonSP
PHB2
NonSP
PHB2
NonSP
PHB2
DsiRNA
αZIKV NS5
αPHB2
αGAPDH
24
48
72
Time (hpi)
C
ZIKV - MOI 0.1
D
ZIKV - MOI 1
E
USUV - MOI 0.1
F
USUV - MOI 1
Log10 virus titre (TCID50/ml)
Time post-infection (h)
G
ZIKV - intracellular
H
ZIKV - extracellular
I
USUV RNA - intracellular
J
USUV RNA - extracellular
Log10 gRNA eq/µg cellular RNA
Log10 gRNA eq/10^4 cells
DsiNSP
DsiPHB2
Multiplicity of infection

Figure 6

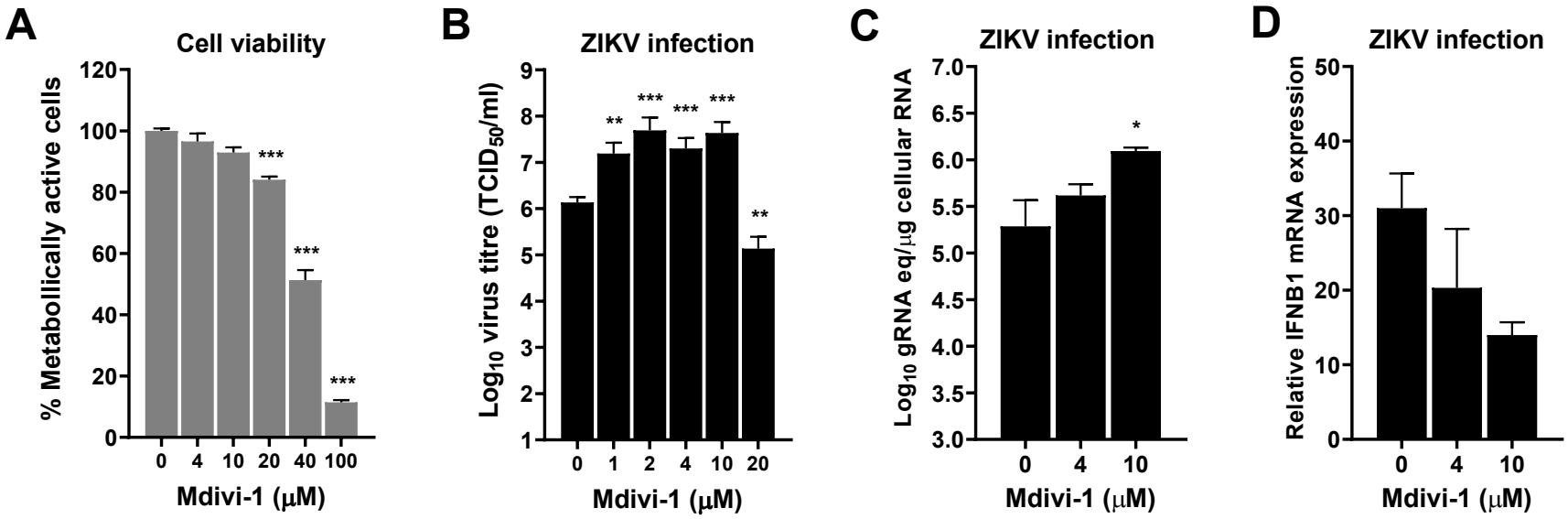
A
Cell viability
% Metabollically active cells
120
100
80
60
40
20
0
***
***
***
0 4 10 20 40 100
Mdivi-1 (μM)
B
ZIKV infection
Log10 virus titre (TCID50/ml)
9
8
7
6
5
4
3
2
1
**
***
***
***
**
0 1 2 4 10 20
Mdivi-1 (μM)
C
ZIKV infection
Log10 gRNA eq/μg cellular RNA
7.0
6.5
6.0
5.5
5.0
4.5
4.0
3.5
3.0
*
0 4 10
Mdivi-1 (μM)
D
ZIKV infection
Relative IFNB1 mRNA expression
50
40
30
20
10
0
0 4 10
Mdivi-1 (μM)

Figure 7

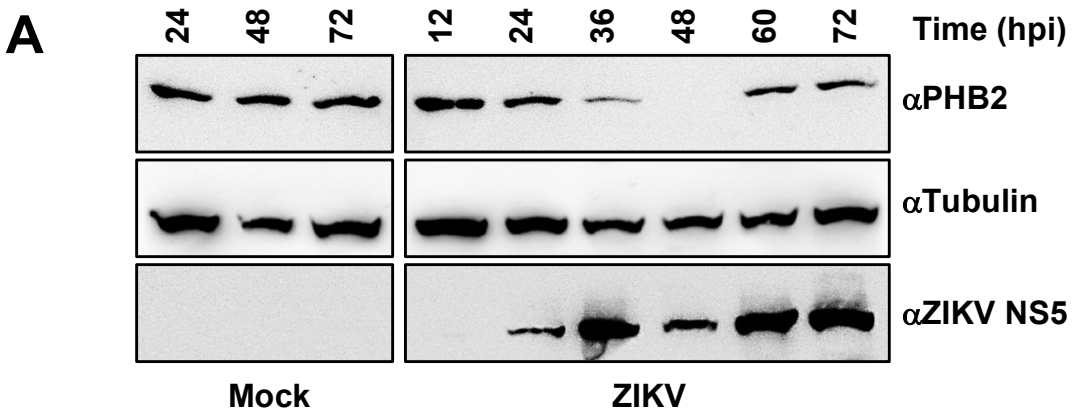
A
24
48
72
12
24
36
48
60
72
Time (hpi)
αPHB2
αTubulin
αZIKV NS5
Mock
ZIKV

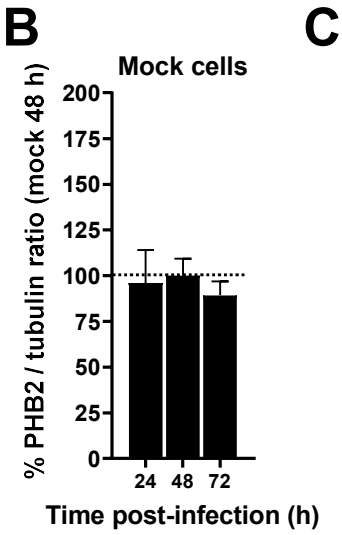
B
Mock cells
% PHB2 / tubulin ratio (mock 48 h)
200
175
150
125
100
75
50
25
0
24 48 72
Time post-infection (h)

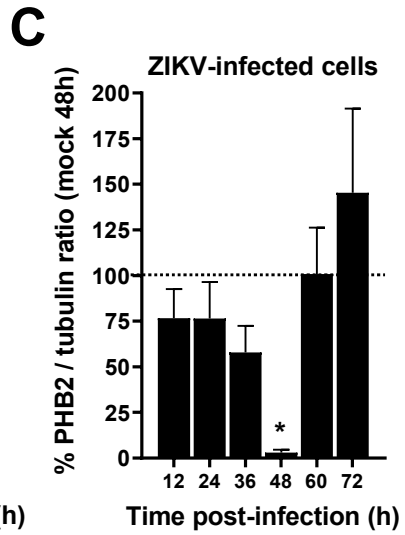
C
ZIKV-infected cells
% PHB2 / tubulin ratio (mock 48h)
200
175
150
125
100
75
50
25
0
*
12 24 36 48 60 72
Time post-infection (h)

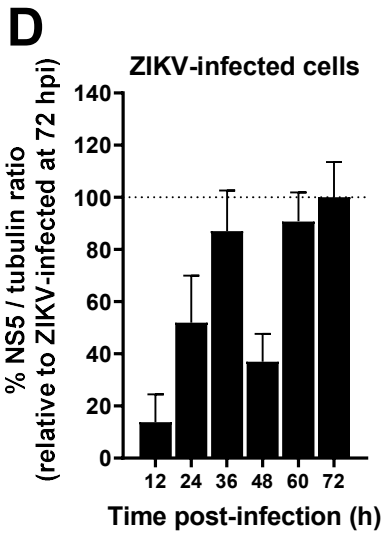
D
ZIKV-infected cells
% NS5 / tubulin ratio
(relative to ZIKV-infected at 72 hpi)
140
120
100
80
60
40
20
0
12 24 36 48 60 72
Time post-infection (h)

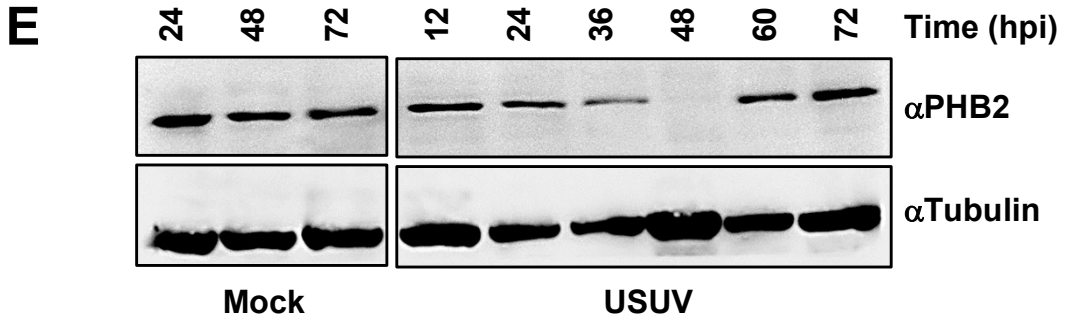
E
24
48
72
12
24
36
48
60
72
Time (hpi)
αPHB2
αTubulin
Mock
USUV

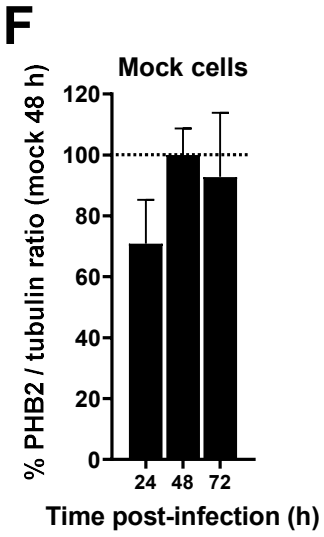
F
Mock cells
% PHB2 / tubulin ratio (mock 48 h)
120
100
80
60
40
20
0
24 48 72
Time post-infection (h)

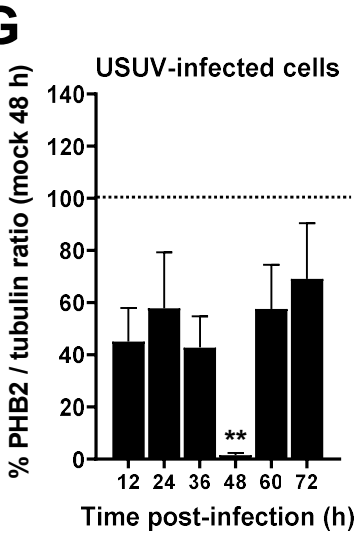
G
USUV-infected cells
% PHB2 / tubulin ratio (mock 48 h)
140
120
100
80
60
40
20
0
**
12 24 36 48 60 72
Time post-infection (h)

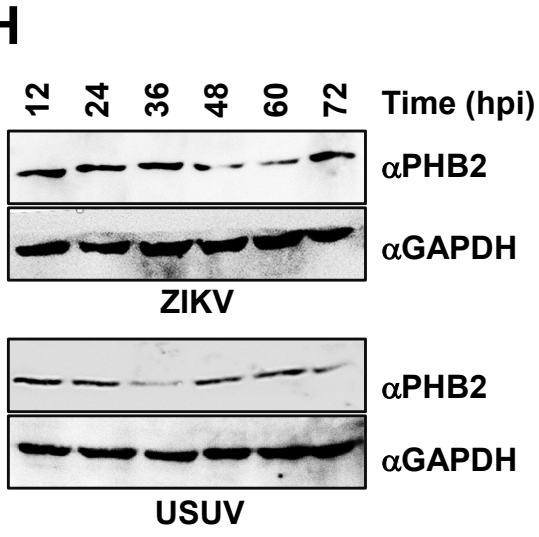
H
12
24
36
48
60
72
Time (hpi)
αPHB2
αGAPDH
ZIKV
αPHB2
αGAPDH
USUV

Figure 8

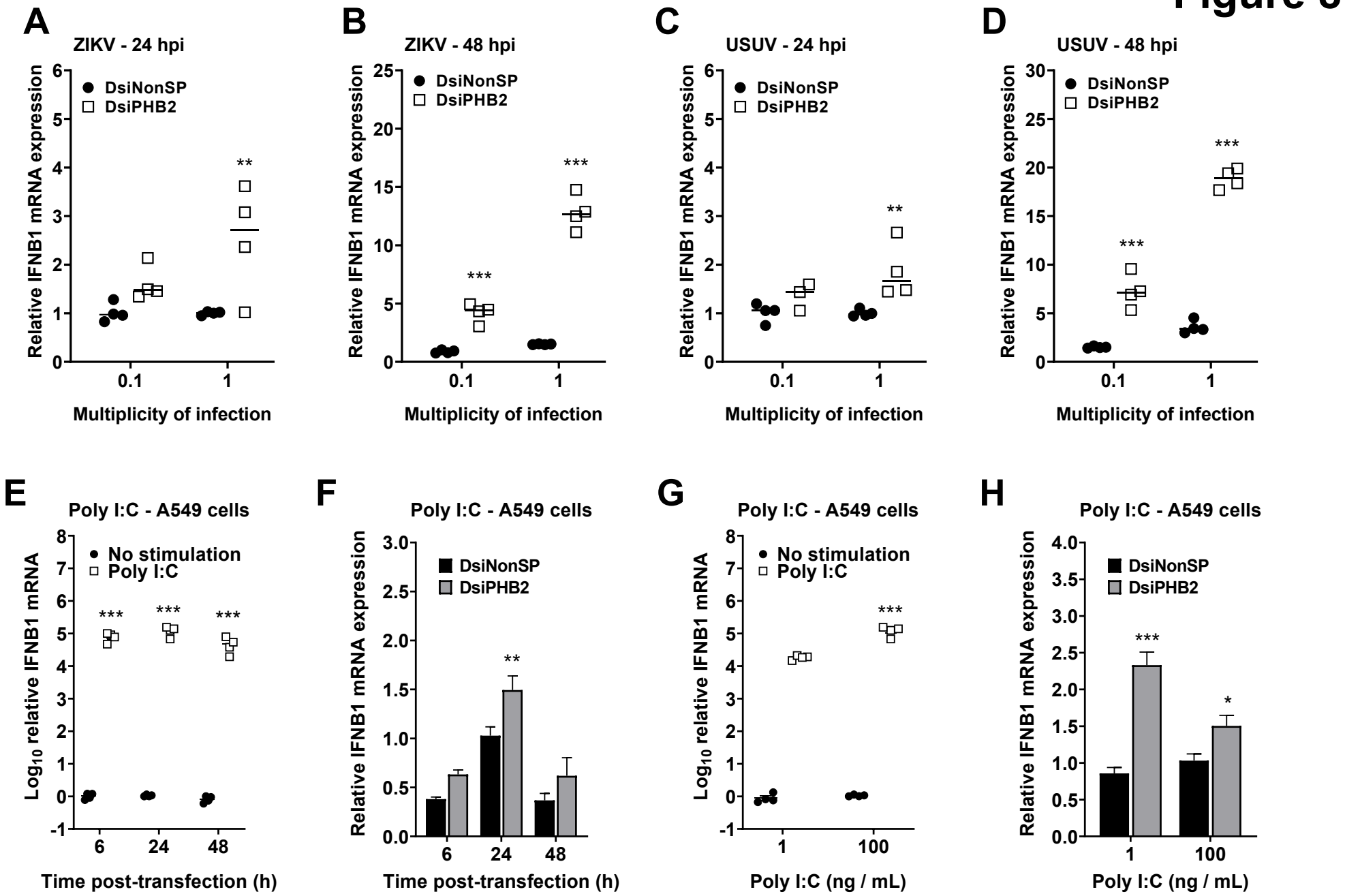
A
ZIKV - 24 hpi
DsiNonSP
DsiPHB2
Relative IFNB1 mRNA expression
Multiplicity of infection
0.1
1
**
B
ZIKV - 48 hpi
DsiNonSP
DsiPHB2
Relative IFNB1 mRNA expression
Multiplicity of infection
0.1
1
***
***
C
USUV - 24 hpi
DsiNonSP
DsiPHB2
Relative IFNB1 mRNA expression
Multiplicity of infection
0.1
1
**
D
USUV - 48 hpi
DsiNonSP
DsiPHB2
Relative IFNB1 mRNA expression
Multiplicity of infection
0.1
1
***
***
E
Poly I:C - A549 cells
No stimulation
Poly I:C
Log10 relative IFNB1 mRNA
Time post-transfection (h)
6
24
48
***
***
***
F
Poly I:C - A549 cells
DsiNonSP
DsiPHB2
Relative IFNB1 mRNA expression
Time post-transfection (h)
6
24
48
**
G
Poly I:C - A549 cells
No stimulation
Poly I:C
Log10 relative IFNB1 mRNA
Poly I:C (ng / mL)
1
100
***
H
Poly I:C - A549 cells
DsiNonSP
DsiPHB2
Relative IFNB1 mRNA expression
Poly I:C (ng / mL)
1
100
***
*

Figure 9

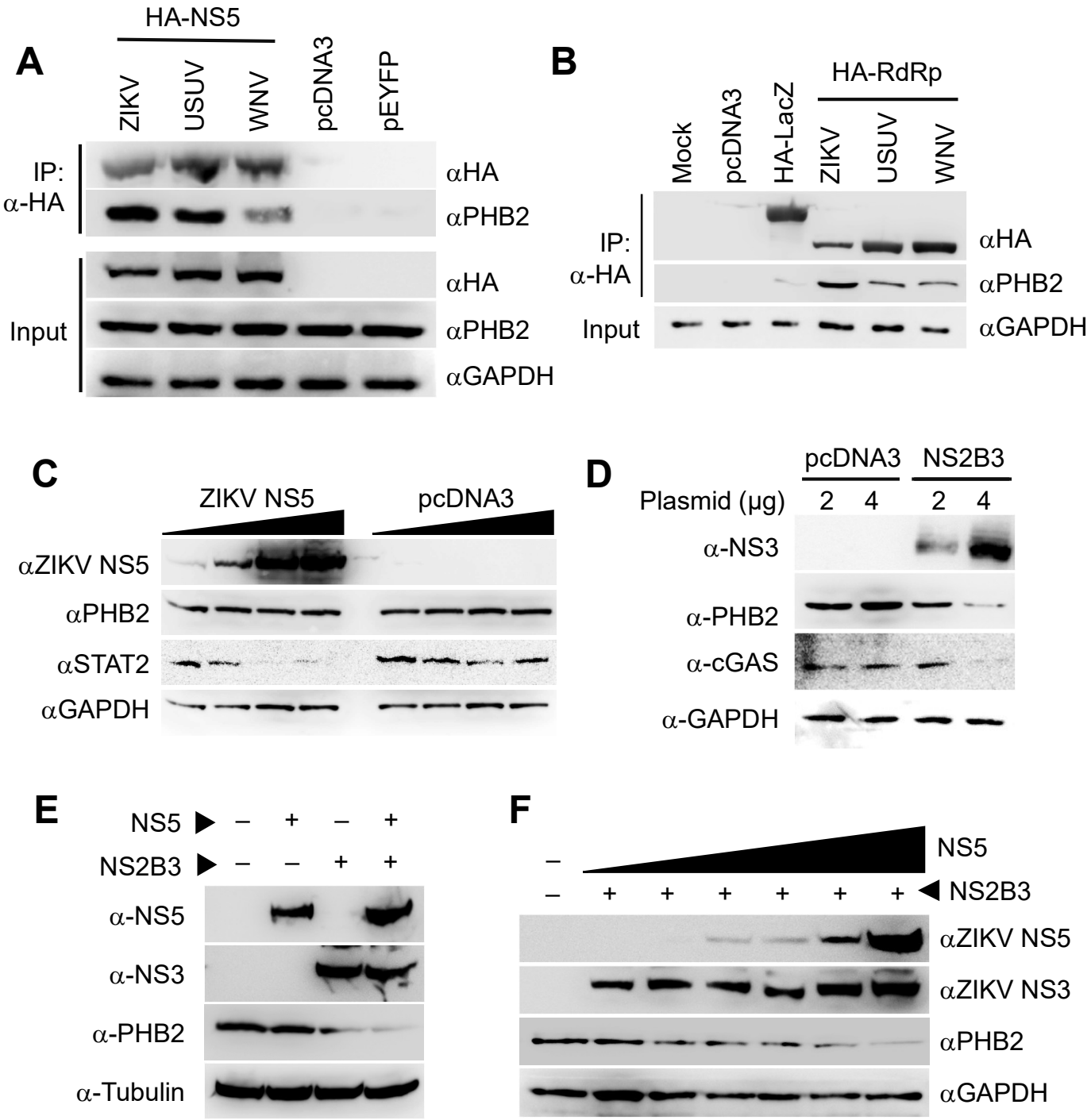
A
HA-NS5
ZIKV
USUV
WNV
pcDNA3
pEYFP
IP:
α-HA
αHA
αPHB2
Input
αHA
αPHB2
αGAPDH
B
HA-RdRp
Mock
pcDNA3
HA-LacZ
ZIKV
USUV
WNV
IP:
α-HA
αHA
αPHB2
Input
αGAPDH
C
ZIKV NS5
pcDNA3
αZIKV NS5
αPHB2
αSTAT2
αGAPDH
D
pcDNA3
NS2B3
Plasmid (μg)
2
4
2
4
α-NS3
α-PHB2
α-cGAS
α-GAPDH
E
NS5
NS2B3
α-NS5
α-NS3
α-PHB2
α-Tubulin
F
NS5
NS2B3
αZIKV NS5
αZIKV NS3
αPHB2
αGAPDH